Computers and Mathematics with Applications 166 (2024) 182–197

Contents lists available at ScienceDirect

Computers and Mathematics with Applications

journal homepage: www.elsevier.com/locate/camwa

Residual-based a posteriori error estimation for mixed virtual element methods

Mauricio Munar [a,*], Andrea Cangiani [b], Iván Velásquez [c]

[a] Departamento de Matemáticas, Facultad de Ciencias Básicas y Aplicadas, Universidad Militar Nueva Granada, Bogotá, Colombia
[b] Scuola Internazionale Superiore di Studi Avanzati - SISSA, Via Bonomea, 265, 34136 Trieste, Italy
[c] Departamento de Ciencias Básicas, Universidad del Sinú Elías Bechara Zainum, Montería, Colombia

ARTICLE INFO

Keywords:
Mixed virtual element method
A posteriori error analysis
Polygonal meshes

ABSTRACT

We present an a posteriori error analysis for the mixed virtual element method (mixed-VEM) applied to general second order elliptic equations. The resulting error estimator is of residual-type. Via the inclusion of a fully local postprocessing of the mixed-VEM solution, we show that the estimator provides a reliable and efficient control on the L^2-norm error between the exact and the postprocessed flux. Numerical examples confirm the theoretical properties of the estimator, and show that it can be effectively used to drive an adaptive mesh refinement algorithm.

1. Introduction

The construction of numerical methods that allow to solve efficiently challenging PDE problems in (possibly moving) complex geometries is a central problem of modern numerical analysis. Enabling the use of general meshes allows numerical methods to better adapt to geometry complexities and solutions anisotropies as typical, for example, of polycrystalline materials modelling [1], material design [23], and discrete fracture networks [2]. Moreover, mesh flexibility can be exploited within adaptive algorithms to improve the resolution of singularities. The first attempts to enable the use of polygonal/polyhedral meshes began in the early '70s from the seminal work of Wachspress [35]. Since then, various approaches have been proposed, including: polygonal FEM [33], mimetic finite differences [7], discontinuous Galerkin methods [14,20], Trefftz finite elements [21], finite elements based on the boundary elements method [32], and recently, virtual elements methods [5,6].

General meshes allow the implementation of adaptive algorithms easily and efficiently as hanging nodes can be simply treated as new nodes and the elements containing them as new polygonal/polyhedral elements. Hence, mesh refinement on polygonal/polyhedral meshes is fully local, in contrast to classical mesh refinement techniques.Recently, several error estimators have been proposed in the context of VEM for primal forms. Firstly, the authors of [8] proposed a posteriori error bounds for the C^1-conforming VEM for the two-dimensional Poisson problem. Next, a posteriori error bounds for the C^0-conforming VEM for the discretization of second-order linear elliptic reaction-convection-diffusion problems with nonconstant coefficients in two and three dimension were proposed in [15], whereas a residual-based a posteriori error estimator for the VEM discretization of the Poisson problem with discontinuous diffusivity coefficient was introduced and analysed in [10]. Additionally, in [30] and [29], the authors developed a posteriori error analysis of a VEM approach for the Steklov eigenvalue problem and the spectral analysis for the elasticity equations, respectively. Other works in this direction can be found in [9,11,17,19,3,37,38,22,28,36]. In particular, the authors of the recent work [22] establish a contraction property for adaptive VEM on standard meshes with hanging nodes. Their comparison with adaptive FEM clearly shows that allowing for multiple hanging nodes yields sharper resolution of steep solution gradients.

In this work we develop an a posteriori error analysis and propose a mesh adaptive strategy for mixed-VEM applied to general second order elliptic problems. We follow the framework proposed in [16,31] to obtain a residual-type estimator which involves fully computable approximations of the flux variable. By expressing the VEM residuals in terms of the postprocessed discrete solution, we are able to prove optimality of the resulting posteriori error estimator in the natural norms. The efficiency of the estimator is also established exploiting the original bubble technique of Verfürth [34] in the polygonal mesh setting [15,30]. The reliability and efficiency of the a posteriori error estimator is confirmed by numerical

* Corresponding author.
E-mail addresses: edgar.munar@unimilitar.edu.co (M. Munar), acangian@sissa.it (A. Cangiani), ivanvelasquez@unisinu.edu.co (I. Velásquez).

https://doi.org/10.1016/j.camwa.2024.05.011
Received 22 August 2023; Received in revised form 21 February 2024; Accepted 7 May 2024

0898-1221/© 2024 The Author(s). Published by Elsevier Ltd. This is an open access article under the CC BY-NC-ND license (http://creativecommons.org/licenses/by-nc-nd/4.0/).

results on both standard and polygonal meshes. We also showcase the use of the estimator to drive a mesh adaptive algorithm. Here we observe that the adaptive algorithm is able to recover optimal convergence of the numerical solution in a series of challenging problems.

The remainder of this paper is organized as follows. In Section 2 we introduce the problem and the associated variational formulation. The Section 3 is dedicated to the mixed virtual element scheme. The a posteriori error analysis of our method, which constitutes the main contribution of this work, is presented in details in Section 4. We introduce an adaptive algorithm and validate its effectiveness with several numerical experiments in Section 5. Finally, in Section 6 we give some concluding remarks.

Throughout the paper, we use the following standard notation. For $\mathcal{O} \subset \mathrm{R}^2$ a bounded domain with polygonal boundary $\partial\mathcal{O}$, we denote by ν the outward unit normal vector to the boundary $\partial\mathcal{O}$. For $s \in \mathrm{R}$, the symbol $|\cdot|_{s,\mathcal{O}}$ stands for the norm of the Hilbertian Sobolev spaces $\mathrm{H}^s(\mathcal{O})$, with the convention $\mathrm{H}^0(\mathcal{O}) := \mathrm{L}^2(\mathcal{O})$. In particular, $\mathrm{H}^{1/2}(\partial\mathcal{O})$ is the trace space on the boundary $\partial\mathcal{O}$ for all functions defined on $\mathrm{H}^1(\mathcal{O})$, and we denote by $\mathrm{H}^{-1/2}(\partial\mathcal{O})$ the dual space of $\mathrm{H}^{1/2}(\partial\mathcal{O})$. Further, we denote by $\langle\cdot,\cdot\rangle$ the duality pairing between $\mathrm{H}^{-1/2}(\partial\mathcal{O})$ and $\mathrm{H}^{1/2}(\partial\mathcal{O})$. For any vector field $\boldsymbol{\tau} = (\tau_i)_{i=1,2}$ and scalar field v, we let

$$\nabla\cdot\boldsymbol{\tau} := \partial_1\tau_1 + \partial_2\tau_2, \quad \mathrm{rot}\,\boldsymbol{\tau} := \partial_1\tau_2 - \partial_2\tau_1, \quad \text{and} \quad \mathbf{rot}\, v := \left(\partial_2 v, -\partial_1 v\right)^{\mathbf{t}}.$$

We recall the Hilbert spaces

$$\mathrm{H}(\mathrm{div};\mathcal{O}) := \left\{ \boldsymbol{\tau} \in [\mathrm{L}^2(\mathcal{O})]^2 : \quad \nabla\cdot\boldsymbol{\tau} \in \mathrm{L}^2(\mathcal{O}) \right\},$$

and

$$\mathrm{H}(\mathrm{rot};\mathcal{O}) := \left\{ \boldsymbol{\tau} \in [\mathrm{L}^2(\mathcal{O})]^2 : \quad \mathrm{rot}\,\boldsymbol{\tau} \in \mathrm{L}^2(\mathcal{O}) \right\},$$

equipped with the usual norms

$$\|\boldsymbol{\tau}\|^2_{\mathrm{div};\mathcal{O}} := \|\boldsymbol{\tau}\|^2_{0,\mathcal{O}} + \|\nabla\cdot\boldsymbol{\tau}\|^2_{0,\mathcal{O}},$$

and

$$\|\boldsymbol{\tau}\|^2_{\mathrm{rot};\mathcal{O}} := \|\boldsymbol{\tau}\|^2_{0,\mathcal{O}} + \|\mathrm{rot}\,\boldsymbol{\tau}\|^2_{0,\mathcal{O}},$$

respectively. We denote by $H := \mathrm{H}(\mathrm{div};\mathcal{O})$ and $Q := \mathrm{L}^2(\mathcal{O})$, whence we can make use of the product space $H \times Q$ endowed with the norm

$$|||(\boldsymbol{\tau}, v)||| := \|\boldsymbol{\tau}\|_{\mathrm{div};\mathcal{O}} + \|v\|_{0,\mathcal{O}}. \tag{1.1}$$

In addition, we will denote with c and C, with or without subscripts, tildes, or hats, generic constants independent of the mesh parameter h, which may take different values in different occurrences.

2. The continuous problem

Let $\Omega \subset \mathrm{R}^2$ be a simply-connected and bounded domain with polygonal boundary $\Gamma := \partial\Omega$. Given $f \in \mathrm{L}^\infty(\Omega)$ and $g \in \mathrm{H}^{-1/2}(\Gamma)$, we consider the problem

$$\begin{aligned} \nabla\cdot(-\boldsymbol{\kappa}(\mathbf{x})\nabla u + \mathbf{b}(\mathbf{x})u) + \gamma(\mathbf{x})u &= f(\mathbf{x}) \quad \text{in} \quad \Omega, \\ u &= g \quad \text{on} \quad \Gamma, \end{aligned} \tag{2.1}$$

where $\gamma \in \mathrm{L}^\infty(\Omega)$, $\mathbf{b} \in [\mathrm{L}^\infty(\Omega)]^2$ and $\boldsymbol{\kappa} \in [\mathrm{L}^\infty(\Omega)]^{2\times 2}$ is a strongly elliptic symmetric diffusion tensor, i.e. there exist $\kappa_*, \kappa^* > 0$, independent of $\mathbf{v}$ and $\mathbf{x}$

$$\kappa_*|\mathbf{v}(\mathbf{x})|^2 \le \mathbf{v}(\mathbf{x})\cdot\boldsymbol{\kappa}(\mathbf{x})\mathbf{v}(\mathbf{x}) \le \kappa^*|\mathbf{v}(\mathbf{x})|^2 \tag{2.2}$$

for almost every $\mathbf{x} \in \Omega$ and for any $\mathbf{v} \in [\mathrm{H}^1_0(\Omega)]^2$, with $|\cdot|$ denoting the standard Euclidean norm on R^2. Now, setting $\boldsymbol{\beta} := \boldsymbol{\kappa}^{-1}\mathbf{b}$ and by introducing the flux variable $\boldsymbol{\sigma} := \boldsymbol{\kappa}(-\nabla u + \boldsymbol{\beta}u)$ in Ω, as an additional unknown, we can rewrite (2.1) as:

$$\boldsymbol{\kappa}^{-1}\boldsymbol{\sigma} = -\nabla u + \boldsymbol{\beta}u \quad \text{in} \quad \Omega, \quad \nabla\cdot\boldsymbol{\sigma} + \gamma u = f \quad \text{in} \quad \Omega, \quad \text{and} \quad u = g \quad \text{on} \quad \Gamma. \tag{2.3}$$

In this way, a mixed variational formulation of (2.3) becomes: find $(\boldsymbol{\sigma}, u) \in H \times Q$ such that

$$\begin{aligned} a((\boldsymbol{\sigma},u),\boldsymbol{\tau}) &= -\langle\boldsymbol{\tau}\cdot\nu, g\rangle \quad \forall\,\boldsymbol{\tau} \in H, \\ b((\boldsymbol{\sigma},u),v) &= (f,v) \quad \forall\, v \in Q, \end{aligned} \tag{2.4}$$

where

$$\begin{aligned} a((\boldsymbol{\sigma},u),\boldsymbol{\tau}) &:= (\boldsymbol{\kappa}^{-1}\boldsymbol{\sigma},\boldsymbol{\tau}) - (u, \nabla\cdot\boldsymbol{\tau} + \boldsymbol{\beta}\cdot\boldsymbol{\tau}), \\ b((\boldsymbol{\sigma},u),v) &:= (v, \nabla\cdot\boldsymbol{\sigma} + \gamma u), \end{aligned} \tag{2.5}$$

which, can be rewritten as: find $(\boldsymbol{\sigma}, u) \in H \times Q$ such that

$$\mathcal{A}((\boldsymbol{\sigma},u),(\boldsymbol{\tau},v)) := a((\boldsymbol{\sigma},u),\boldsymbol{\tau}) + b((\boldsymbol{\sigma},u),v) = \mathcal{F}(\boldsymbol{\tau},v), \qquad \forall\,(\boldsymbol{\tau},v) \in H \times Q, \tag{2.6}$$

with

$$\mathcal{F}(\boldsymbol{\tau}, v) := (f, v) - \langle \boldsymbol{\tau} \cdot \nu, g \rangle, \tag{2.7}$$

for all $(\boldsymbol{\tau}, v) \in H \times Q$. Under the assumptions on data the existence and uniqueness of the weak solution of (2.6) is guaranteed (see [6]).

3. The virtual element method

Throughout the paper we consider $\{\mathcal{T}_h\}_{h>0}$ as a family of decomposition of Ω into open non-overlapping polygonal elements. For each polygon K and each edge e of $\mathcal{T}_h$, we denote their diameters by h_K and h_e, respectively, whereas $h := \max_{K \in \mathcal{T}_h} h_K$. We further let $\mathcal{E}_h = \mathcal{E}_h(\Omega) \cup \mathcal{E}_h(\Gamma)$ be the set of all edges of $\mathcal{T}_h$, where $\mathcal{E}_h(\Omega) := \left\{ e \in \mathcal{E}_h : \quad e \subseteq \overline{\Omega} \right\}$ and $\mathcal{E}_h(\Gamma) := \left\{ e \in \mathcal{E}_h : \quad e \subseteq \Gamma \right\}$ and denote by $\mathcal{E}(K) \subset \mathcal{E}_h$ the set of edges of any $K \in \mathcal{T}_h$. Given an edge $e \in \mathcal{E}_h$, we let h_e be its length and we fix a unit normal vector $\nu_e := (\nu_1, \nu_2)^{\mathbf{t}}$ and let $s_e := (-\nu_2, \nu_1)^{\mathbf{t}}$ be the corresponding unit tangential vector along e. However, when no confusion arises, we simply write ν and s instead of ν_e and s_e, respectively. Finally, given $\boldsymbol{\zeta} \in [\mathrm{L}^2(\Omega)]^2$, for each $K \in \mathcal{T}_h$ and $e \in \mathcal{E}_h(\Omega) \cap \mathcal{E}(K)$ we denote by $[\![\boldsymbol{\zeta} \cdot s]\!]$ the tangential jump of $\boldsymbol{\zeta}$ across e, that is $[\![\boldsymbol{\zeta} \cdot s]\!] := (\boldsymbol{\zeta}\big|_K - \boldsymbol{\zeta}\big|_{K'})\big|_e \cdot s$, where K and K' are the elements in $\mathcal{T}_h$ sharing e as a common edge.

We use the following standard mesh-regularity assumptions. The sequence of meshes $\{\mathcal{T}_h\}_{h>0}$ is such there exists a positive constant ρ such that: i) all $K \in \mathcal{T}_h$ is star-shaped with respect to a ball of radius ρh_K, and ii) for all $K \in \mathcal{T}_h$ and all $e \in \partial K$ we have that $h_e \geq \rho h_K$. These assumptions imply that each $K \in \mathcal{T}_h$ is simply connected and the numbers of edges of each $K \in \mathcal{T}_h$ are bounded above by a positive constant, which is depending only on ρ. Moreover, assumption i) implies that K admits a sub-triangulation $\mathcal{T}_h^K$ resulting from the joining of all vertices of K with a point with respect to which K is starred. Furthermore, due to both assumption i) and ii), the resulting global triangulation $\widehat{\mathcal{T}_h} := \bigcup_{K \in \mathcal{T}_h} \mathcal{T}_h^K$ is shape-regular.

Given an integer $\ell \geq 0$ and $\mathcal{O} \subseteq \mathrm{R}^2$, we denote by $\mathrm{P}_\ell(\mathcal{O})$ the space of polynomials on $\mathcal{O}$ of degree up to ℓ. In addition, given an edge $e \in \mathcal{T}_h$ with barycentre x_e and diameter h_e, we denote the following set of $(\ell + 1)$ normalized monomials on e

$$\mathcal{B}_\ell(e) := \left\{ \left(\frac{x - x_e}{h_e} \right)^j \right\}_{0 \leq j \leq \ell},$$

which certainly constitutes a basis on $\mathrm{P}_\ell(e)$. Similarly, on $K \in \mathcal{T}_h$ with barycentre $\mathbf{x}_K$, we define the following set of $\frac{1}{2}(\ell + 1)(\ell + 2)$ normalized monomials

$$\mathcal{B}_\ell(K) := \left\{ \left(\frac{\mathbf{x} - \mathbf{x}_K}{h_K} \right)^{\boldsymbol{\alpha}} \right\}_{0 \leq |\boldsymbol{\alpha}| \leq \ell},$$

which is a basis of $\mathrm{P}_\ell(K)$. Notice that in the definition of $\mathcal{B}_\ell(K)$ above, we made use of the multi-index notation, that is, given $\mathbf{x} := (x_1, x_2)^{\mathbf{t}} \in \mathrm{R}^2$ and $\boldsymbol{\alpha} := (\alpha_1, \alpha_2)^{\mathbf{t}}$, with non-negative integers α_1, α_2, we set $\mathbf{x}^{\boldsymbol{\alpha}} := x_1^{\alpha_1} x_2^{\alpha_2}$ and $|\boldsymbol{\alpha}| := \alpha_1 + \alpha_2$. We further let $\mathcal{G}_\ell(K)$ be a basis of $\left(\nabla \mathrm{P}_{\ell+1}(K)\right) \cap [\mathrm{P}_\ell(K)]^2$, whereas with $\mathcal{G}_\ell^\perp(K)$ we denote a basis of the $[\mathrm{L}^2(K)]^2$-orthogonal space of $\mathcal{G}_\ell(K)$ in $[\mathrm{P}_\ell(K)]^2$.

Hereinafter, we denote by $\Pi_k^{\mathcal{O}} : \mathrm{L}^2(\mathcal{O}) \to \mathrm{P}_k(\mathcal{O})$ the $\mathrm{L}^2(\mathcal{O})$-orthogonal projection onto the space $\mathrm{P}_k(\mathcal{O})$, for any $\mathcal{O} \subseteq \mathrm{R}^2$ and $k \geq 0$. In this sense, $\mathcal{O}$ can be a line segment or polygon of $\mathcal{T}_h$. We remark here that to ensure consistency with the author's previous work (see [15,31]), we are using the same notation for the orthogonal projector onto a line segment or polygon of $\mathcal{T}_h$, even over the whole domain. In addition, we will make use of a vectorial version of the aforementioned projector, which is denoted by $\boldsymbol{\Pi}_k^0$. The following approximation properties of these projectors are well-known:

$$\|v - \Pi_k^0(v)\|_{0,K} \leq C h_K^m |v|_{m,K} \quad \text{and} \quad \|\boldsymbol{\tau} - \boldsymbol{\Pi}_k^0(\boldsymbol{\tau})\|_{0,K} \leq C h_K^m |\boldsymbol{\tau}|_{m,K} \tag{3.1}$$

for all $K \in \mathcal{T}_h$, and for all $v \in \mathrm{H}^m(K)$, $\boldsymbol{\tau} \in [\mathrm{H}^m(K)]^2$, with $m \in \{0, 1, \ldots, k+1\}$; see e.g. [12].

3.1. Virtual element spaces and approximation properties

Following [6], given $k \geq 0$ and $K \in \mathcal{T}_h$, we define the local space

$$\begin{aligned} H_h^K := \Big\{ \boldsymbol{\tau} \in \mathrm{H}(\mathrm{div}; K) \cap \mathrm{H}(\mathrm{rot}; K) : \quad & \boldsymbol{\tau} \cdot \nu|_e \in \mathrm{P}_k(e) \quad \forall \text{ edge } e \in \partial K, \\ & \nabla \cdot \boldsymbol{\tau} \in \mathrm{P}_k(K) \quad \text{and} \quad \mathrm{rot}\, \boldsymbol{\tau} \in \mathrm{P}_{k-1}(K) \Big\}. \end{aligned} \tag{3.2}$$

which is characterised by the following unisolvent [6, Section 3] local degrees of freedom:

$$\begin{aligned} &\int_e q\,(\boldsymbol{\tau} \cdot \nu) \quad \forall\, q \in \mathcal{B}_k(e), && \forall \text{ edge } e \in \mathcal{T}_h, \\ &\int_K \boldsymbol{\tau} \cdot \nabla q \quad \forall\, q \in \mathcal{B}_k(K) \setminus \{1\}, && \forall\, K \in \mathcal{T}_h, \\ &\int_K \boldsymbol{\tau} \cdot \eta \quad \forall\, \eta \in \mathcal{G}_k^\perp(K), && \forall\, K \in \mathcal{T}_h. \end{aligned} \tag{3.3}$$

For each $\boldsymbol{\tau} \in [\mathrm{H}^1(K)]^2$ we denote by $\boldsymbol{\tau}_I \in H_h^K$ the Lagrange interpolant of $\boldsymbol{\tau}$ with respect to the local degrees of freedom defined on (3.3). It is easy to see that $\nabla \cdot \boldsymbol{\tau}_I = \Pi_k^0(\nabla \cdot \boldsymbol{\tau})$. Hence, for each $\boldsymbol{\tau} \in [\mathrm{H}^1(K)]^2$ such that $\nabla \cdot \boldsymbol{\tau} \in \mathrm{H}^r(K)$, with $r \in \{0, \ldots, k+1\}$, it holds (see [6])

$$\|\boldsymbol{\tau}-\boldsymbol{\tau}_I\|_{\mathrm{div};K} \leq C\, h_K^r \left\{ |\boldsymbol{\tau}|_{r,K} + |\nabla\cdot\boldsymbol{\tau}|_{r,K} \right\} \qquad \forall\, K\in\mathcal{T}_h\,. \tag{3.4}$$

Additionally, for each $\boldsymbol{\tau}\in[\mathrm{H}^1(\Omega)]^2$ we can deduce that

$$\|(\boldsymbol{\tau}-\boldsymbol{\tau}_I)\cdot\nu\|_{0,e} \leq C\, h_e^{1/2}\|\boldsymbol{\tau}\|_{1,K} \qquad \forall \text{ edge } e\in\mathcal{T}_h\,, \tag{3.5}$$

for any $K\in\mathcal{T}_h$ having e as an edge. This result follows by introducing $\overline{\boldsymbol{\tau}}_K$ as the mean of $\boldsymbol{\tau}$ over K and using the standard arguments [12], yielding

$$\begin{aligned}
\|(\boldsymbol{\tau}-\boldsymbol{\tau}_I)\cdot\nu\|_{0,e} &= \|\boldsymbol{\tau}\cdot\nu-\Pi_k^0(\boldsymbol{\tau}\cdot\nu)\|_{0,e}\\
&= \|(\boldsymbol{\tau}-\overline{\boldsymbol{\tau}}_K)\cdot\nu-\Pi_k^0((\boldsymbol{\tau}-\overline{\boldsymbol{\tau}}_K)\cdot\nu)\|_{0,e}\\
&\leq \|(\boldsymbol{\tau}-\overline{\boldsymbol{\tau}}_K)\cdot\nu\|_{0,e}\\
&\leq C\left(h_e^{-1/2}\|\boldsymbol{\tau}-\overline{\boldsymbol{\tau}}_K\|_{0,K}+h_e^{1/2}|\boldsymbol{\tau}-\overline{\boldsymbol{\tau}}_K|_{1,K}\right)\\
&\leq C\, h_e^{1/2}\|\boldsymbol{\tau}\|_{1,K}\,.
\end{aligned}$$

Finally, the global space is constructed from the above local spaces as

$$H_h := \left\{ \boldsymbol{\tau}\in H : \quad \boldsymbol{\tau}\Big|_K \in H_h^K \quad \forall\, K\in\mathcal{T}_h \right\}, \tag{3.6}$$

with the global degrees of freedom are obtained by collecting the local ones. For the space Q is enough to take

$$Q_h := \left\{ v\in Q : \quad v\Big|_K \in Q_k^K := \mathrm{P}_k(K) \quad \forall\, K\in\mathcal{T}_h \right\}. \tag{3.7}$$

3.2. The discrete scheme and a priori error estimates

Here we use a slight modification of the discrete formulation proposed in [6, Section 3.4]. Indeed, using the fact that the degrees of freedom introduced in (3.3) allow the explicit computation of the projector $\boldsymbol{\Pi}_k^0$ for each $\boldsymbol{\tau}\in H_h^K$ (cf. [6, Section 3.2]), we define the local bilinear form

$$\begin{aligned}
a_h^K((\boldsymbol{\sigma}_h,u_h),\boldsymbol{\tau}_h) &= (\boldsymbol{\kappa}^{-1}\boldsymbol{\Pi}_k^0(\boldsymbol{\sigma}_h),\boldsymbol{\Pi}_k^0(\boldsymbol{\tau}_h))+S^K(\boldsymbol{\sigma}_h-\boldsymbol{\Pi}_k^0(\boldsymbol{\sigma}_h),\boldsymbol{\tau}_h-\boldsymbol{\Pi}_k^0(\boldsymbol{\tau}_h))\\
&\quad -(u_h,\nabla\cdot\boldsymbol{\tau}_h+\boldsymbol{\beta}\cdot\boldsymbol{\Pi}_k^0(\boldsymbol{\tau}_h)) \quad \forall\boldsymbol{\sigma}_h,\boldsymbol{\tau}_h\in H_h, u_h\in Q_h,
\end{aligned} \tag{3.8}$$

where $S^K : H_h^K\times H_h^K\to\mathrm{R}$ is any symmetric and positive definite bilinear form such that there exist constants α_*, $\alpha^*>0$ depending only on ρ, such that

$$\alpha_*\|\boldsymbol{\zeta}_h\|_{0,K}\leq S^K(\boldsymbol{\zeta}_h,\boldsymbol{\zeta}_h) \leq \alpha^*\|\boldsymbol{\zeta}_h\|_{0,K} \qquad \forall\,\boldsymbol{\zeta}_h\in H_h^K, \quad \text{with} \quad \boldsymbol{\Pi}_k^0(\boldsymbol{\zeta}_h)=0\,. \tag{3.9}$$

In turn, denoting by a_h the respective global bilinear form corresponding to the sum of all contributions of the local forms a_h^K we get the discrete formulation: find $(\boldsymbol{\sigma}_h,u_h)\in H_h\times Q_h$ such that

$$\begin{aligned}
a_h((\boldsymbol{\sigma}_h,u_h),\boldsymbol{\tau}_h) &= -\langle\boldsymbol{\tau}_h\cdot\nu,g\rangle \qquad \forall\,\boldsymbol{\tau}_h\in H_h,\\
b((\boldsymbol{\sigma}_h,u_h),v_h) &= (f,v_h) \qquad \forall\, v_h\in Q_h\,.
\end{aligned} \tag{3.10}$$

The inconsistency between a and a_h is established by the following lemma.

Lemma 3.1. *There holds*

$$\begin{aligned}
|(a-a_h)((\boldsymbol{\sigma}_h,u_h),\boldsymbol{\tau}_h)| \leq C\sum_{K\in\mathcal{T}_h}\Big\{ &\|\boldsymbol{\kappa}^{-1}\boldsymbol{\Pi}_k^0(\boldsymbol{\sigma}_h)-\boldsymbol{\Pi}_k^0(\boldsymbol{\kappa}^{-1}\boldsymbol{\Pi}_k^0(\boldsymbol{\sigma}_h))\|_{0,K}+\|\boldsymbol{\beta}u_h-\boldsymbol{\Pi}_k^0(\boldsymbol{\beta}u_h)\|_{0,K}\\
&+S^K(\boldsymbol{\sigma}_h-\boldsymbol{\Pi}_k^0(\boldsymbol{\sigma}_h),\boldsymbol{\sigma}_h-\boldsymbol{\Pi}_k^0(\boldsymbol{\sigma}_h))\Big\}\|\boldsymbol{\tau}_h\|_{0,K}
\end{aligned}$$

Proof. The proof is a slight modification of [6, Section 4.2]. □

Now, analogously to the continuous case, we introduce the global bilinear form $\mathcal{A}_h$ given by:

$$\mathcal{A}_h((\boldsymbol{\sigma}_h,u_h),(\boldsymbol{\tau}_h,v_h)) := a_h((\boldsymbol{\sigma}_h,u_h)+b((\boldsymbol{\sigma}_h,u_h),v_h) \qquad \forall\,(\boldsymbol{\sigma}_h,u_h),(\boldsymbol{\tau}_h,v_h)\in H_h\times Q_h\,. \tag{3.11}$$

Therefore, the mixed virtual element scheme associated with the formulation (2.6) reads: find $(\boldsymbol{\sigma}_h,u_h)\in H_h\times Q_h$ such that

$$\mathcal{A}_h((\boldsymbol{\sigma}_h,u_h),(\boldsymbol{\tau}_h,v_h))=\mathcal{F}(\boldsymbol{\tau}_h,v_h), \qquad \forall\,(\boldsymbol{\tau}_h,v_h)\in H_h\times Q_h\,. \tag{3.12}$$

It is straightforward to show that the problem (3.12) has a unique solution (see [6, Section 3.3]). And the following optimal a priori error estimates were established in [6, Theorem 4.1].

Theorem 3.1. *Let $(\boldsymbol{\sigma},u)\in H\times Q$ and $(\boldsymbol{\sigma}_h,u_h)\in H_h\times Q_h$ be the unique solutions of the continuous and discrete schemes (2.6) and (3.12), respectively. Assume that for some $s\in[1,k+1]$ there hold $\boldsymbol{\sigma}\Big|_K\in[\mathrm{H}^s(K)]^2$, and $\nabla\cdot\boldsymbol{\sigma}\in\mathrm{H}^s(K)$ for each $K\in\mathcal{T}_h$. Then, there exists $C>0$, independent of h, such that*

$$|||(\boldsymbol{\sigma},u)-(\boldsymbol{\sigma}_h,u_h)||| \leq Ch^s \sum_{K\in\mathcal{T}_h}\left\{|\boldsymbol{\sigma}|_{s,K}+|\nabla\cdot\boldsymbol{\sigma}|_{s,K}+|u|_{s,K}\right\}. \tag{3.13}$$

Next, as usual for the VEM, it is necessary to get error estimates for computable approximations of the virtual solution. To this end, we construct an approximation from the virtual solution $\boldsymbol{\sigma}_h$, which is computed locally. This is obtained as its $[\mathrm{L}^2(K)]^2$-orthogonal projection on $[\mathrm{P}_k(K)]^2$, namely $\boldsymbol{\Pi}_k^0(\boldsymbol{\sigma}_h), \forall\, K\in\mathcal{T}_h$. We remark here that this approximation of $\boldsymbol{\sigma}_h$ can be explicitly computed for each $K\in\mathcal{T}_h$ using only its degrees of freedom (c.f. (3.3)). See [13, Section 5.3] for the details. Their convergence properties are established by the following result.

Theorem 3.2. *Let $(\boldsymbol{\sigma},u)\in H\times Q$ and $(\boldsymbol{\sigma}_h,u_h)\in H_h\times Q_h$ be the unique solutions of the continuous and discrete schemes (2.6) and (3.12), respectively. Assume that for some $s\in[1,k+1]$ there hold $\boldsymbol{\sigma}\big|_K\in[\mathrm{H}^s(K)]^2$, and $\nabla\cdot\boldsymbol{\sigma}\big|_K\in\mathrm{H}^s(K)$ for each $K\in\mathcal{T}_h$. In addition, let $\boldsymbol{\Pi}_k^0(\boldsymbol{\sigma}_h)$ be the discrete approximation introduced above. Then, there exists a positive constant C, independent of h, such that*

$$\|(\boldsymbol{\sigma},u)-(\boldsymbol{\Pi}_k^0(\boldsymbol{\sigma}_h),u_h)\|_{0,\Omega} \leq C\,h^s \sum_{K\in\mathcal{T}_h}\left\{|\boldsymbol{\sigma}|_{s,K}+|\nabla\cdot\boldsymbol{\sigma}|_{s,K}+|u|_{s,K}\right\},$$

Proof. The proof is based in a slight modification of Theorem 4.3 in [27]. □

4. A posteriori error analysis

In this section we present the a posteriori error analysis of the mixed virtual element scheme (3.12). We follow the approach from [16], which allows us to establish an adaptive strategy in terms of the approximation of $\boldsymbol{\sigma}_h$ introduced in Section 3.2.

Let $(\boldsymbol{\sigma}_h,u_h)\in H_h\times Q_h$ be the unique solution of (3.12). In addition, let $\boldsymbol{\Pi}_k^0(\boldsymbol{\sigma}_h)$ be the discrete approximation introduced in Section 3.2. Then, we define for each $K\in\mathcal{T}_h$ the local a posteriori error indicators

$$\Psi_K^2 := \sum_{i=1}^{4}\Psi_{i,K}^2,$$

and

$$\begin{aligned}\theta_K^2 :=\ & h_K^2\|\boldsymbol{\kappa}^{-1}\boldsymbol{\Pi}_k^0(\boldsymbol{\sigma}_h)+\nabla u_h-\boldsymbol{\beta}u_h\|_{0,K}^2+h_K^2\|\mathrm{rot}\left(\boldsymbol{\kappa}^{-1}\boldsymbol{\Pi}_k^0(\boldsymbol{\sigma}_h)-\boldsymbol{\beta}u_h\right)\|_{0,K}^2\\ &+\sum_{e\in\mathcal{E}(K)\cap\mathcal{E}_h(\Omega)}h_e\left\{\|[\![u_h]\!]\|_{0,e}^2+\left\|[\![\left(\boldsymbol{\kappa}^{-1}\boldsymbol{\Pi}_k^0(\boldsymbol{\sigma}_h)-\boldsymbol{\beta}u_h\right)\cdot s]\!]\right\|_{0,e}^2\right\}\\ &+\sum_{e\in\mathcal{E}(K)\cap\mathcal{E}_h(\Gamma)}h_e\left\{\|u_h-g\|_{0,e}^2+\left\|\left(\boldsymbol{\kappa}^{-1}\boldsymbol{\Pi}_k^0(\boldsymbol{\sigma}_h)-\boldsymbol{\beta}u_h\right)\cdot s-\frac{dg}{ds}\right\|_{0,e}^2\right\},\end{aligned} \tag{4.1}$$

where

$$\begin{aligned}\Psi_{1,K}^2 &:= \|f-\nabla\cdot\boldsymbol{\sigma}_h-\gamma u_h\|_{0,K}^2, & \Psi_{2,K}^2 &:= S^K(\boldsymbol{\sigma}_h-\boldsymbol{\Pi}_k^0(\boldsymbol{\sigma}_h),\boldsymbol{\sigma}_h-\boldsymbol{\Pi}_k^0(\boldsymbol{\sigma}_h)),\\ \Psi_{3,K}^2 &:= \|\boldsymbol{\beta}u_h-\boldsymbol{\Pi}_k^0(\boldsymbol{\beta}u_h)\|_{0,K}^2, & \Psi_{4,K}^2 &:= \|\boldsymbol{\kappa}^{-1}\boldsymbol{\Pi}_k^0(\boldsymbol{\sigma}_h)-\boldsymbol{\Pi}_k^0(\boldsymbol{\kappa}^{-1}\boldsymbol{\Pi}_k^0(\boldsymbol{\sigma}_h))\|_{0,K}^2.\end{aligned} \tag{4.2}$$

We observe that the term $\frac{dg}{ds}$ in θ_K^2 requires more regularity in the trace g. In particular, we need that $g\in H^1(\Gamma)$ (see [27]). Then, we introduce the global error estimator given by

$$\boldsymbol{\eta} := \left\{\sum_{K\in\mathcal{T}_h}\left\{\Psi_K^2+\theta_K^2\right\}\right\}^{1/2}. \tag{4.3}$$

Now, making suitable assumptions on the data, we can deduce the following estimates, which constitutes the main results of this section.

Theorem 4.1. *Let $(\boldsymbol{\sigma},u)\in H\times Q$ and $(\boldsymbol{\sigma}_h,u_h)\in H_h\times Q_h$ be the unique solutions of (2.6) and (3.10), respectively. Moreover, let $\boldsymbol{\Pi}_k^0(\boldsymbol{\sigma}_h)$ be the postprocessed solution from $\boldsymbol{\sigma}_h$. Then, if the Dirichlet datum $g\in H^1(\Gamma)$, there holds*

$$|||(\boldsymbol{\sigma},u)-(\boldsymbol{\sigma}_h,u_h)|||+\|\boldsymbol{\sigma}-\boldsymbol{\Pi}_k^0(\boldsymbol{\sigma}_h)\|_{0,\Omega} \leq C_{\mathrm{rel}}\boldsymbol{\eta}. \tag{4.4}$$

Moreover, if $(\kappa^{-1}\boldsymbol{\Pi}_k^0(\boldsymbol{\sigma}_h)-\boldsymbol{\beta}u_h)|_K$, $((\kappa^{-1}\boldsymbol{\Pi}_k^0(\boldsymbol{\sigma}_h)-\boldsymbol{\beta}u_h)\cdot s)|_{\widetilde{e}}$ and $\left(\boldsymbol{\kappa}^{-1}\boldsymbol{\Pi}_k^0(\boldsymbol{\sigma}_h)-\boldsymbol{\beta}u_h\right)\cdot s-\frac{dg}{ds}|_e$ are piecewise polynomials for each $K\in\mathcal{T}_h$, $\widetilde{e}\in\mathcal{E}_h(\Omega)$ and $e\in\mathcal{E}_h(\Gamma)$, respectively, we have

$$\begin{aligned}C_{\mathrm{eff}}\boldsymbol{\eta} \leq\ & |||(\boldsymbol{\sigma},u)-(\boldsymbol{\sigma}_h,u_h)|||+\|\boldsymbol{\sigma}-\boldsymbol{\Pi}_k^0(\boldsymbol{\sigma}_h)\|_{0,\Omega},+\|\boldsymbol{\beta}u-\boldsymbol{\Pi}_k^0(\boldsymbol{\beta}u)\|_{0,\Omega}\\ &+\|\boldsymbol{\kappa}^{-1}\boldsymbol{\sigma}-\boldsymbol{\Pi}_k^0(\boldsymbol{\kappa}^{-1}\boldsymbol{\sigma})\|_{0,\Omega}+\|\boldsymbol{\sigma}-\boldsymbol{\Pi}_k^0(\boldsymbol{\sigma})\|_{0,\Omega}\end{aligned} \tag{4.5}$$

The constants $C_{\mathrm{rel}},C_{\mathrm{eff}}>0$ are independent of h.

Remark 4.2. In Theorem 4.1, the assumptions on the data are required to facilitate the computations of the efficiency estimates. Moreover, there is no restriction on the polynomial degree (see for instance [16, Section 5.4] for further details).

The rest of this section is devoted to the proof of the above results. In particular, in Section 4.1 we prove that $\boldsymbol{\eta}$ satisfies the reliability property (4.4), whereas the corresponding efficiency property (4.5) is derived in Section 4.2. Overall, Theorem 4.1 encapsulates lower and upper bounds for the global error estimator defined in (4.3) in terms of the discrete approximation $\boldsymbol{\Pi}_k^0(\boldsymbol{\sigma}_h)$.

4.1. Upper bound

In this section we proceed as in [31, Section 3.1]. Specifically, we make use of the interpolation operator $\mathcal{I}_k^h : \mathrm{H}^1(\Omega) \to V_k^h$, where V_k^h is the original C^0-conforming virtual element space of order k from [5]. Namely, for all $k \geq 0$, we let

$$V_k^h := \left\{ v \in \mathrm{H}^1(\Omega) : \Delta v \in \mathrm{P}_{k-1}(K) \quad \text{and} \quad v\Big|_{\partial K} \in \mathbb{B}_k(\partial K) \quad \forall K \in \mathcal{T}_h \right\},$$

with

$$\mathbb{B}_k(\partial K) := \left\{ v \in \mathrm{C}(\partial K) : \quad v|_e \in \mathrm{P}_{k+1}(e) \quad \forall e \in \mathcal{E}(K) \right\}.$$

We recall here that the interpolation operator $\mathcal{I}_k^h$ is such that, for each $v \in \mathrm{H}^1(\Omega)$, there holds

$$m_j(v - \mathcal{I}_k^h(v)) = 0 \quad \forall\, j = 1, \ldots, \dim V_k^h,$$

where $\{m_j(v)\}_j^{\dim V_k^h}$ collects the degrees of freedom of v. For more details see [5, Section 4.4]. The following lemma establishes the local approximation properties of $\mathcal{I}_h$.

Lemma 4.1. *There exist constants $c_1, c_2 > 0$, independent of h, such that for all $v \in \mathrm{H}^1(\Omega)$ there hold*

$$\|v - \mathcal{I}_k^h(v)\|_{0,K} \leq c_1 h_K \|v\|_{1,\omega_K} \qquad \forall\, K \in \mathcal{T}_h, \tag{4.6}$$

and

$$\|(v - \mathcal{I}_k^h(v)) \cdot \nu_e\|_{0,e} \leq c_2 h_e^{1/2} \|v\|_{1,\omega_e} \qquad \forall\, e \in \mathcal{E}_h, \tag{4.7}$$

where $\omega_K := \{K' \in \mathcal{T}_h : \ K \cap K' \neq \emptyset\}$ and $\omega_e := \{K \in \mathcal{T}_h : \ e \in \mathcal{E}(K)\}$.

Proof. See [30, Section 4, Proposition 4.2] and [31, Lemma 3.2]. □

Remark. Given $k \geq 0$, $v \in V_k^h$ and $K \in \mathcal{T}_h$, there hold $\mathrm{rot}(\mathbf{rot}\, v)\Big|_K = -\Delta v\Big|_K \in \mathrm{P}_{k-1}(K)$ and $(\mathbf{rot}\, v)\nu\Big|_e = (\nabla v)s\Big|_e \in \mathrm{P}_k(e)$ for all edge $e \in \partial K$. Therefore, from (3.2) we can deduce that $\mathbf{rot}\, v\Big|_K \in H_k^K$ for all $K \in \mathcal{T}_h$. For more details, see [31, Remark 1].

Lemma 4.2. *Given $(\boldsymbol{\sigma}, u) \in H \times Q$ and $(\boldsymbol{\sigma}_h, u_h) \in H_h \times Q_h$ the unique solutions of (2.6) and (3.12), respectively, define $e_{\boldsymbol{\sigma}} := \boldsymbol{\sigma} - \boldsymbol{\sigma}_h$ and $e_u = u - u_h$. There exists a positive constant $\widetilde{C}$, independent of h, such that*

$$\widetilde{C} |||(e_{\boldsymbol{\sigma}}, e_u)||| \leq \boldsymbol{\eta}. \tag{4.8}$$

Proof. From the well-posedness of the variational formulation (2.6), we know that $\mathcal{A}$ induces an isomorphism. In particular, there exists a positive constant C, such that, for all $(\boldsymbol{\rho}, w) \in H \times Q$, it holds

$$C |||(\boldsymbol{\rho}, w)||| \leq \sup_{\substack{(\boldsymbol{\tau}, v) \in H \times Q \\ (\boldsymbol{\tau}, v) \neq \mathbf{0}}} \frac{\mathcal{A}((\boldsymbol{\rho}, w), (\boldsymbol{\tau}, v))}{\|(\boldsymbol{\tau}, v)\|_{H \times Q}}. \tag{4.9}$$

In particular, taking $(\boldsymbol{\rho}, w) := (e_{\boldsymbol{\sigma}}, e_u)$, we have that

$$\begin{aligned} \mathcal{A}((\boldsymbol{\rho}, w), (\boldsymbol{\tau}, v)) &= a((e_{\boldsymbol{\sigma}}, e_u), \boldsymbol{\tau}) + b((e_{\boldsymbol{\sigma}}, e_u), v) \\ &= a((e_{\boldsymbol{\sigma}}, e_u), \boldsymbol{\tau}) + (v, f - \nabla \cdot \boldsymbol{\sigma}_h - \gamma u_h), \end{aligned}$$

and replacing the foregoing expression into (4.9), we get

$$C |||(\boldsymbol{\sigma}, u) - (\boldsymbol{\sigma}_h, u_h)||| \leq \|f - \nabla \cdot \boldsymbol{\sigma}_h - \gamma u_h\|_Q + \sup_{\substack{\boldsymbol{\tau} \in H \\ \boldsymbol{\tau} \neq \mathbf{0}}} \frac{a((e_{\boldsymbol{\sigma}}, e_u), \boldsymbol{\tau})}{\|\boldsymbol{\tau}\|_H}. \tag{4.10}$$

Notice that for any $\boldsymbol{\tau}, \boldsymbol{\tau}_h \in H$ there holds

$$\begin{aligned} a((e_\sigma, e_u), \boldsymbol{\tau}) &= -\langle \boldsymbol{\tau} \cdot \nu, g \rangle - a((\boldsymbol{\sigma}_h, u_h), \boldsymbol{\tau}) \\ &= -\langle (\boldsymbol{\tau} - \boldsymbol{\tau}_h) \cdot \nu, g \rangle - a((\boldsymbol{\sigma}_h, u_h), \boldsymbol{\tau}) + a_h((\boldsymbol{\sigma}_h, u_h), \boldsymbol{\tau}_h) \\ &= -\langle (\boldsymbol{\tau} - \boldsymbol{\tau}_h) \cdot \nu, g \rangle - a((\boldsymbol{\sigma}_h, u_h), \boldsymbol{\tau} - \boldsymbol{\tau}_h) - (a - a_h)((\boldsymbol{\sigma}_h, u_h), \boldsymbol{\tau}_h) \\ &= I + II \end{aligned}$$

with

$$I := -\langle (\boldsymbol{\tau} - \boldsymbol{\tau}_h)\cdot\nu, g\rangle - a((\boldsymbol{\sigma}_h, u_h), \boldsymbol{\tau} - \boldsymbol{\tau}_h),$$

$$II := -(a - a_h)((\boldsymbol{\sigma}_h, u_h), \boldsymbol{\tau}_h).$$

We fix $\boldsymbol{\tau}_h \in H_h$ using the Helmholtz decomposition of $\boldsymbol{\tau}$. Namely, given $\boldsymbol{\tau} \in H$, we have the decomposition $\boldsymbol{\tau} = \boldsymbol{\zeta} + \mathbf{rot}\,\varphi$, with $\boldsymbol{\zeta} \in [\mathrm{H}^1(\Omega)]^2$ and $\varphi \in \mathrm{H}^1(\Omega)$, owing to the assumption that Ω is simply connected. Then, denoting by $\widetilde{\varphi} := \mathcal{I}_k^h(\varphi)$ and recalling that $\boldsymbol{\zeta}_I$ is the Lagrange interpolant of $\boldsymbol{\zeta}$, we can take $\boldsymbol{\tau}_h := \boldsymbol{\zeta}_I + \mathbf{rot}\,\widetilde{\varphi} \in H_h$, whence its possible deduce that $\boldsymbol{\tau} - \boldsymbol{\tau}_h = \boldsymbol{\zeta} - \boldsymbol{\zeta}_I + \mathbf{rot}\,(\varphi - \widetilde{\varphi})$. We observe that from Lemma 3.1 and the fact that $\|\boldsymbol{\tau}_h\|_Q \leq C\|\boldsymbol{\tau}\|_H$ for some positive constant C independent of $\boldsymbol{\tau}$ we can deduce

$$II \leq C\left\{\sum_{K\in\mathcal{T}_h} \Psi_{2,K}^2 + \Psi_{3,K}^2 + \Psi_{4,K}^2\right\}^{1/2} \|\boldsymbol{\tau}\|_H, \tag{4.11}$$

whereas, to bound II, we can integrate by parts on each $K \in \mathcal{T}_h$. Indeed, by using that $\mathbf{rot}(\varphi - \widetilde{\varphi})\cdot\nu = \dfrac{d}{ds}(\varphi - \widetilde{\varphi})$, noting that $\dfrac{dg}{ds} \in \mathrm{L}^2(\Gamma)$, and following similar arguments to the proof of Lemma 5.4 in [25], in join with Lemma 4.1, and the fact that the number of elements in ω_e is bounded, we can deduce that

$$I \leq C\left\{\sum_{K\in\mathcal{T}_h} \theta_K^2\right\}^{1/2} \|\boldsymbol{\tau}\|_H. \tag{4.12}$$

Finally, from (4.10)-(4.12) the proof is completed. □

From the result in the above Lemma 4.2, using the triangle inequality and the lower bound in (3.9) the upper bound (4.4) readily follows.

4.2. Lower bound

In this section we derive suitable upper bounds for our estimator, starting with the terms defining the local error indicators (4.2). The following results are obtained using standard bounding arguments in Sobolev spaces and the properties of the orthogonal projector $\boldsymbol{\Pi}_k^0$. More precisely, applying the Cauchy-Schwartz inequality, the polynomial consistency of $\boldsymbol{\Pi}_k^0$, and the stability of the bilinear form $S^K(\cdot,\cdot)$ (cf. (3.9)). Therefore, we omit the proof (see [31, Section 3.2] for further details).

$$\begin{aligned}
\Psi_{1,K}^2 &\leq C_\gamma\left\{\|\nabla\cdot(\boldsymbol{\sigma} - \boldsymbol{\sigma}_h)\|_{0,K}^2 + \|u - u_h\|_{0,K}^2\right\}\\
\Psi_{2,K}^2 &\leq C_{\alpha^*}\left\{\|\boldsymbol{\sigma} - \boldsymbol{\sigma}_h\|_{0,K}^2 + \|\boldsymbol{\sigma} - \boldsymbol{\Pi}_k^0(\boldsymbol{\sigma})\|_{0,K}^2\right\}\\
\Psi_{3,K}^2 &\leq C_\beta\left\{\|u - u_h\|_{0,K}^2 + \|\boldsymbol{\beta}u - \boldsymbol{\Pi}_k^0(\boldsymbol{\beta}u)\|_{0,K}^2\right\}\\
\Psi_{4,K}^2 &\leq C_{\boldsymbol{\kappa},\alpha^*}\left\{\|\boldsymbol{\sigma} - \boldsymbol{\sigma}_h\|_{0,K}^2 + \|\boldsymbol{\sigma} - \boldsymbol{\Pi}_k^0(\boldsymbol{\sigma})\|_{0,K}^2 + \|\boldsymbol{\kappa}^{-1}\boldsymbol{\sigma} - \boldsymbol{\Pi}_k^0(\boldsymbol{\kappa}^{-1}\boldsymbol{\sigma})\|_{0,K}^2\right\},
\end{aligned}$$

where the constants only depend of the data. Therefore, we have

$$\begin{aligned}
C\left\{\sum_{K\in\mathcal{T}_h} \Psi_K^2\right\}^{1/2} \leq\ & |||(\boldsymbol{\sigma}, u) - (\boldsymbol{\sigma}_h, u_h)||| + \|\boldsymbol{\sigma} - \boldsymbol{\Pi}_k^0(\boldsymbol{\sigma}_h)\|_{0,\Omega} + \|\boldsymbol{\beta}u - \boldsymbol{\Pi}_k^0(\boldsymbol{\beta}u)\|_{0,\Omega}\\
&+\|\boldsymbol{\kappa}^{-1}\boldsymbol{\sigma} - \boldsymbol{\Pi}_k^0(\boldsymbol{\kappa}^{-1}\boldsymbol{\sigma})\|_{0,\Omega} + \|\boldsymbol{\sigma} - \boldsymbol{\Pi}_k^0(\boldsymbol{\sigma})\|_{0,\Omega}
\end{aligned} \tag{4.13}$$

The upper bounds of the terms (4.1) which depend on the mesh parameters h_K and h_e, will be derived next. To this end, we make use of the techniques based on bubble functions, extension operators, and discrete trace and inverse inequalities introduced by [34]; and used for the analysis of the VEM in primal form in [15,30]. More precisely, the analysis is based on the following properties, see [15,30] for more details. Given $k \geq 0$ and $K \in \mathcal{T}_h$, there exists a positive constant C_{bub} independent of h_K such that

$$C_{\mathrm{bub}}^{-1}\|q\|_{0,K}^2 \leq \|\psi_K^{1/2}q\|_{0,K}^2 \leq C_{\mathrm{bub}}\|q\|_{0,K}^2 \qquad \forall\, q \in \mathrm{P}_k(K), \tag{4.14}$$

and

$$C_{\mathrm{bub}}^{-1}\|q\|_{0,K} \leq \|\psi_K q\|_{0,K} + h_K|\psi_K q|_{1,K} \leq C_{\mathrm{bub}}\|q\|_{0,K} \qquad \forall\, q \in \mathrm{P}_k(K). \tag{4.15}$$

In addition, given $e \in \partial K$, there hold

$$C_{\mathrm{bub}}^{-1}\|q\|_{0,e}^2 \leq \|\psi_e^{1/2}q\|_{0,e}^2 \leq C_{\mathrm{bub}}\|q\|_{0,e}^2 \qquad \forall\, q \in \mathrm{P}_k(e), \tag{4.16}$$

and

$$h_K^{-1/2}\|\psi_e L(q)\|_{0,K} + h_K^{1/2}|\psi_e L(q)|_{1,K} \leq C_{\mathrm{bub}}\|q\|_{0,e} \qquad \forall\, q \in \mathrm{P}_k(e), \tag{4.17}$$

for any $K \in \omega_e$, the patch of elements sharing e as an edge.

In the forthcoming derivation, we require for simplicity the further assumption that some terms are locally polynomials as in the statement of Theorem 4.1. Otherwise, further higher order terms, given by the errors arising from suitable polynomial approximations, will appear in the bounds below. Here, the respective terms can be interpreted as data oscillation terms of high order, which are usual in the context of residual a posteriori analysis of finite elements. The next result is inspired by the results proven in [16, Section 5.4].

Lemma 4.3. *There exist some constants $C_i > 0$, $i = 1, \ldots, 4$, independent of h, such that*

$$\begin{aligned}
h_K^2 \|\kappa^{-1}\boldsymbol{\Pi}_k^0(\boldsymbol{\sigma}_h) + \nabla u_h - \boldsymbol{\beta} u_h\|_{0,K}^2 &\leq C_1 \left\{ h_K^2 \|\boldsymbol{\sigma} - \boldsymbol{\Pi}_k^0(\boldsymbol{\sigma}_h)\|_{0,K}^2 + \|u - u_h\|_{0,K}^2 \right\} \\
h_K^2 \|\mathrm{rot}\left(\kappa^{-1}\boldsymbol{\Pi}_k^0(\boldsymbol{\sigma}_h) - \boldsymbol{\beta} u_h\right)\|_{0,K}^2 &\leq C_2 \left\{ \|\boldsymbol{\sigma} - \boldsymbol{\Pi}_k^0(\boldsymbol{\sigma}_h)\|_{0,K}^2 + \|u - u_h\|_{0,K}^2 \right\} \\
h_{\widetilde{e}} \left\{ \|[\![u_h]\!]\|_{0,\widetilde{e}}^2 + \left\| [\![\left(\kappa^{-1}\boldsymbol{\Pi}_k^0(\boldsymbol{\sigma}_h) - \boldsymbol{\beta} u_h\right) \cdot s]\!] \right\|_{0,\widetilde{e}}^2 \right\} &\leq C_3 \left\{ \|\boldsymbol{\sigma} - \boldsymbol{\Pi}_k^0(\boldsymbol{\sigma}_h)\|_{0,\omega_{\widetilde{e}}}^2 + \|u - u_h\|_{0,\omega_{\widetilde{e}}}^2 \right\} \\
h_e \left\{ \|u_h - g\|_{0,e}^2 + \left\| \left(\kappa^{-1}\boldsymbol{\Pi}_k^0(\boldsymbol{\sigma}_h) - \boldsymbol{\beta} u_h\right) \cdot s - \frac{dg}{ds} \right\|_{0,e}^2 \right\} &\leq C_4 \left\{ \|\boldsymbol{\sigma} - \boldsymbol{\Pi}_k^0(\boldsymbol{\sigma}_h)\|_{0,\omega_e}^2 + \|u - u_h\|_{0,\omega_e}^2 \right\}
\end{aligned}$$

for $K \in \mathcal{T}_h$, $\widetilde{e} \in \mathcal{E}_h(\Omega)$ and $e \in \mathcal{E}_h(\Gamma)$, where $\omega_{\widetilde{e}}$ and ω_e are as in Lemma 4.1.

Proof. The first and second estimates are slight modifications of the proofs in the Lemma 6.3 of [18] (see also Lemma 5.5 in [24]) and Lemma 4.3 of [4], respectively. Here we make use the fact that $\left(\kappa^{-1}\boldsymbol{\Pi}_k^0(\boldsymbol{\sigma}_h) - \boldsymbol{\beta} u_h\right)\Big|_K$ is polynomial in each $K \in \mathcal{T}_h$. The idea is based in integration by parts, the Cauchy-Schwarz inequality and the estimate (4.15). The third estimate is consequence of using the same arguments of the Lemma 4.4 of [4] in join with the second inequality of the present Lemma and the estimate (4.17). Finally, for the last estimate, we proceed as in the proof of Lemmas 4.14 and 4.15 of [26] (see also Lemma 5.7 in [24]). Here we use the fact that $\left(\kappa^{-1}\boldsymbol{\Pi}_k^0(\boldsymbol{\sigma}_h) - \boldsymbol{\beta} u_h\right) \cdot s - \frac{dg}{ds}\Big|_e$ and the data g are polynomials for each $e \in \mathcal{E}_h(\Gamma)$. □

From the above Lemma we thus get

$$C \left\{ \sum_{K \in \mathcal{T}_h} \theta_K^2 \right\}^{1/2} \leq \|u - u_h\|_{0,\Omega} + \|\boldsymbol{\sigma} - \boldsymbol{\Pi}_k^0(\boldsymbol{\sigma}_h)\|_{0,\Omega}, \tag{4.18}$$

and the lower bound (4.5) immediately follows from estimates (4.13) and (4.18).

5. Numerical tests

In this section we present several numerical tests confirming the reliability and efficiency of the a posteriori error estimator $\boldsymbol{\eta}$ derived in Section 4. Moreover, we showcase the behaviour of a mesh adaptive algorithm driven $\boldsymbol{\eta}$. In what follows, N stands for the total number of degrees of freedom of (3.12). The initial meshes used in the tests are shown in Fig. 5.1. The individual errors are defined by

$$\begin{aligned}
\mathtt{e}(\boldsymbol{\sigma}) &:= \|\boldsymbol{\sigma} - \boldsymbol{\Pi}_k^0(\boldsymbol{\sigma}_h)\|_{0,\Omega} + \|\mathrm{div}(\boldsymbol{\sigma}) - \mathrm{div}(\boldsymbol{\sigma}_h)\|_{0,\Omega}, \qquad \mathtt{e}(u) := \|u - u_h\|_{0,\Omega}, \\
\mathtt{e}(\boldsymbol{\sigma}, u) &:= \left\{ [\mathtt{e}(\boldsymbol{\sigma})]^2 + [\mathtt{e}(u)]^2 \right\}^{1/2},
\end{aligned} \tag{5.1}$$

whereas the effectivity index with respect the estimator $\boldsymbol{\eta}$ is given by

$$\mathtt{eff}(\boldsymbol{\eta}) := \frac{\mathtt{e}(\boldsymbol{\sigma}, u)}{\boldsymbol{\eta}}.$$

Observe that this quantity is not a true efficiency index due we are not using exactly the norm defined in (1.1) when evaluate the error, however, it gives information on the behaviour of $\boldsymbol{\eta}$. Moreover, in this case, some of the local indicators defined in (4.2) can be interpreted as oscillation terms. At least they must have the same rate of convergence of the global error if the exact solution is smooth enough (see, e.g. [31]). In Test 1 it is proved numerically. Then, we define the experimental rates of convergence

$$\mathtt{r}(\cdot) := -2 \frac{\log(\mathtt{e}(\cdot)/\mathtt{e}'(\cdot))}{\log(N/N')},$$

where $\mathtt{e}$ and $\mathtt{e}'$ denote the corresponding errors for two consecutive meshes with N and N' the respective degrees of freedom of each decomposition. Similarly, we define:

$$\mathtt{r}(\Psi_i) := -2 \frac{\log(\Psi_i/\Psi_i')}{\log(N/N')},$$

where $\Psi_i := \left\{ \sum_{K \in \mathcal{T}_h} \Psi_{i,K}^2 \right\}^{1/2}$. For the numerical tests that include adaptivity, we use for the local a posteriori error indicator $\boldsymbol{\eta}_K := \boldsymbol{\eta}|_K$, the following strategy:

(i) Start with a coarse mesh $\mathcal{T}_h$.
(ii) Solve the discrete problem on the current mesh $\mathcal{T}_h$.

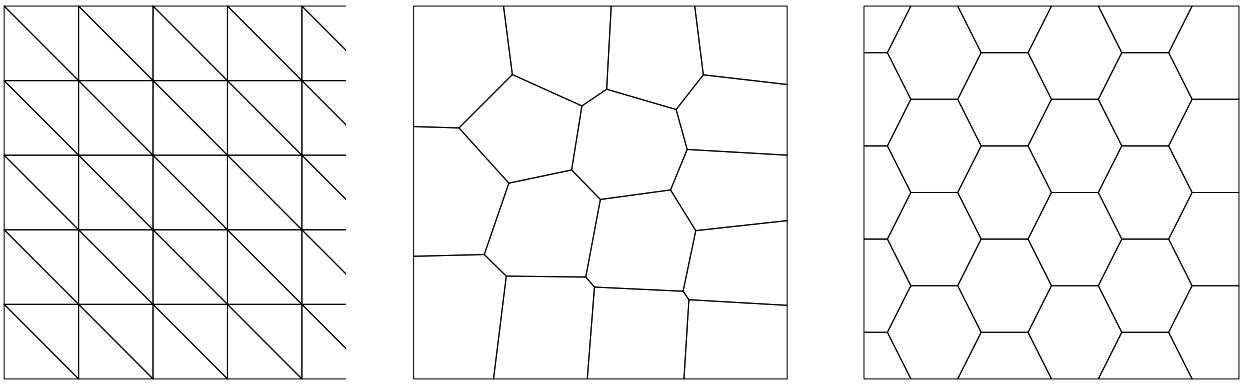

Fig. 5.1. Sample meshes: triangular, Voronoi and hexagonal.

Table 5.1
Test 1. Convergence history for a uniformly generated sequence of triangular meshes.

k	N	$\mathtt{e}(\boldsymbol{\sigma})$	$\mathtt{r}(\boldsymbol{\sigma})$	$\mathtt{e}(u)$	$\mathtt{r}(u)$	$\mathtt{e}(\boldsymbol{\sigma},u)$	$\mathtt{r}(\boldsymbol{\sigma},u)$	$\boldsymbol{\eta}$	$\mathtt{r}(\boldsymbol{\eta})$	$\mathtt{eff}(\boldsymbol{\eta})$
0	520	1.7098e+00	−−	5.4985e-02	−−	1.7107e+00	−−	2.1587e+00	−−	0.7925
	2040	8.5776e-01	1.0093	2.6519e-02	1.0670	8.5817e-01	1.0094	1.0983e+00	0.9888	0.7814
	8080	4.2924e-01	1.0059	1.3133e-02	1.0211	4.2944e-01	1.0060	5.5295e-01	0.9971	0.7766
	32160	2.1466e-01	1.0033	6.5503e-03	1.0071	2.1476e-01	1.0033	2.7730e-01	0.9993	0.7745
1	1840	1.2471e-01	−−	3.3052e-03	−−	1.2475e-01	−−	1.7170e-01	−−	0.7266
	7280	3.1265e-02	2.0118	8.0405e-04	2.0556	3.1275e-02	2.0118	4.3026e-02	2.0124	0.7270
	28960	7.8225e-03	2.0068	1.9957e-04	2.0184	7.8250e-03	2.0068	1.0763e-02	2.0071	0.7270
	115520	1.9561e-03	2.0037	4.9802e-05	2.0066	1.9567e-03	2.0037	2.6913e-03	2.0037	0.7271
2	3760	5.6988e-03	−−	1.4757e-04	−−	5.7007e-03	−−	1.1591e-02	−−	0.4918
	14920	7.1462e-04	3.0128	1.7870e-05	3.0635	7.1484e-04	3.0128	1.4569e-03	3.0094	0.4907
	59440	8.9399e-05	3.0076	2.2151e-06	3.0209	8.9426e-05	3.0076	1.8247e-04	3.0060	0.4901
	237280	1.1177e-05	3.0041	2.7630e-07	3.0074	1.1180e-05	3.0041	2.2825e-05	3.0033	0.4898

(iii) Compute local indicators for each $K \in \mathcal{T}_h$.
(iv) Mark each $K' \in \mathcal{T}_h$ to be refined applying the rule

$$\boldsymbol{\eta}_{K'} \geq \beta \max_{K\in\mathcal{T}_h} \boldsymbol{\eta}_K,$$

with $\beta \in (0,1)$. We refine the mesh by connecting the midpoint of each edge of polygon K (to be refined) with its barycentre. For more details, see [15, Section 6.2]. For the tests 1 to 3 we use $\beta = 0.5$ whereas for the test 4 we use $\beta = 0.5$ for $k = 0$ and $\beta = 0.7$ for $k = 1, 2$.
(v) Define the new mesh as actual mesh $\mathcal{T}_h$ and go to step (ii).

5.1. Test 1. Smooth solution: behaviour of the estimator under uniform refinement

For this first test we consider $\Omega := (0,1)^2$ with data

$$\boldsymbol{\kappa} = \begin{pmatrix} y^2+1 & -xy \\ -xy & x^2+1 \end{pmatrix}, \quad \mathbf{b} = \begin{pmatrix} x \\ y \end{pmatrix}, \quad \text{and} \quad \gamma = x^2 + y^3,$$

whereas the source term f is such that the exact solution is given by

$$u(x,y) = \sin(\pi x)\sin(\pi y).$$

The aim of this test is to verify the asymptotic behaviour of the estimator with a smooth solution and under uniform refinements. To this end, we use two families of uniformly generated meshes: uniform triangular and hexagonal. The corresponding coarsest meshes are shown in Fig. 5.1. Table 5.1 show the convergence history of the errors and the estimator on the two sequence of uniformly refined meshes, indicating that all converge at the optimal rate for polynomial degrees $k = 0, 1, 2$. The robustness of the estimator with respect to the mesh shape is clearly confirmed. Further, the effectivity is bounded below in each case. Additionally, we observe from Fig. 5.2 that each indicator Ψ_i for $i = 1, ..., 4$, converges with optimal order $k + 1$.

5.2. Test 2. Uniform and adaptive refinement: interior layer

For this test we consider $\Omega := (0,1)^2$ with data $\boldsymbol{\kappa} = \begin{pmatrix} 1 & 0 \\ 0 & 1 \end{pmatrix}$, $\mathbf{b} = \begin{pmatrix} x \\ y \end{pmatrix}$ and $\gamma = \sin(2\pi x)\sin(2\pi y)$, whereas the source term f is such that the exact solution is given by

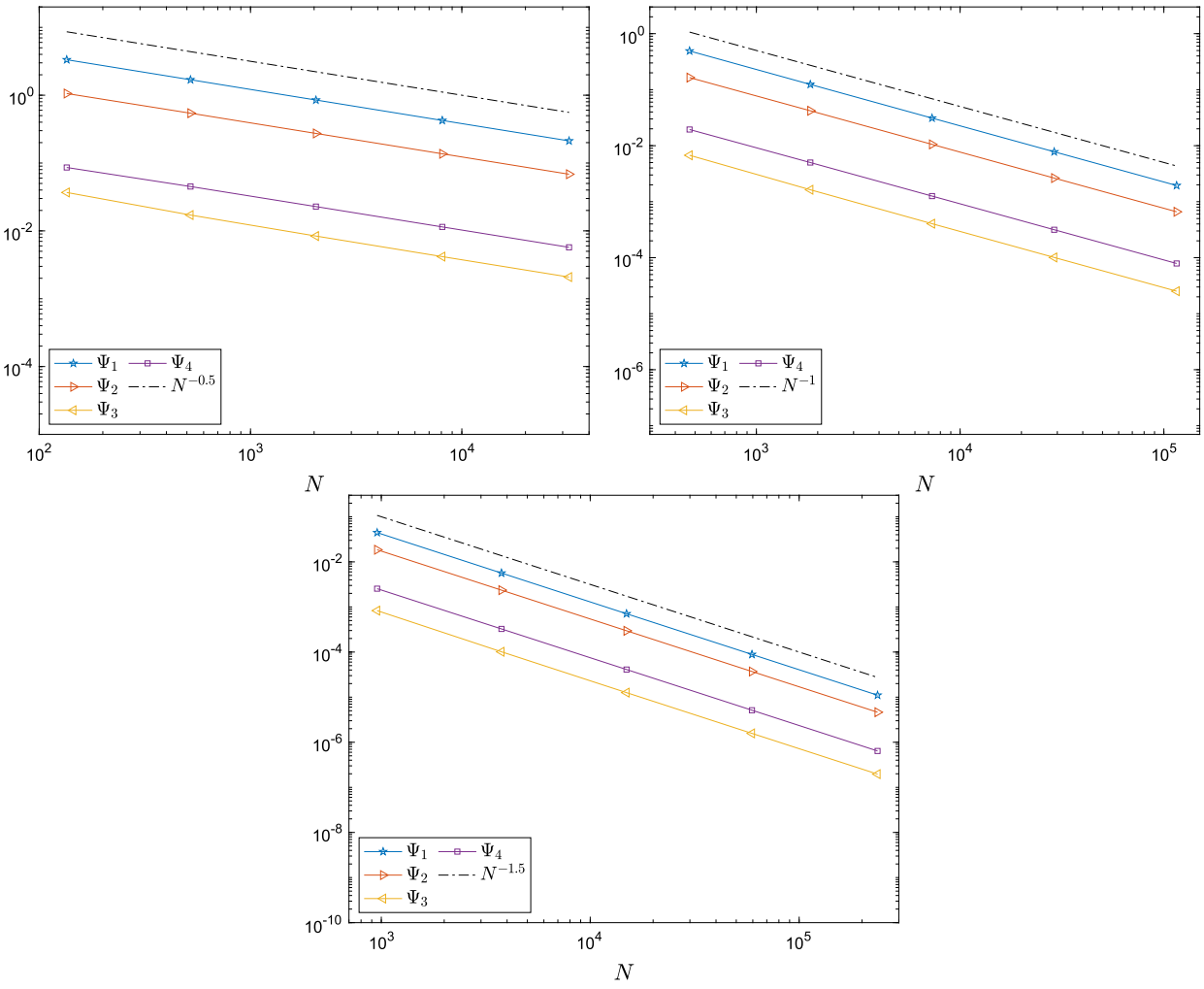

Fig. 5.2. Test 1. Convergence history of some terms using a uniformly generated sequence of triangular meshes for $k = 0$ (top-left), $k = 1$ (top-right) and $k = 2$ (bottom).

$$u(x, y) = 16x(1 - y)y(1 - x)\arctan(25x - 100y + 50).$$

The main difficulty of Test 2 is the presence of an interior sharp layer which is completely unresolved by the initial mesh. To test the good properties of our estimator in this challenging context, we chose an initial mesh to consist of triangles which are not aligned with the interior layer. The exact solution is showed in the Fig. 5.3 where can be evidenced the interior layer above mentioned. The convergence history of the mesh adaptive algorithm is reported in Fig. 5.4 together with the results obtained with uniform convergence for comparison. As expected, adaptive refinement reaches the optimal convergence rate much faster than uniform refinement. Further, from Fig. 5.4 it is possible verify that the effectivity index remains bounded from above and below, thus confirming the reliability and efficiency of the estimator for the associated adaptive algorithm as well. In Fig. 5.5 we also observe that the orders of convergence of the estimator are consistent for each polynomial order. Finally, Fig. 5.6 shows sample meshes from the sequence produced by the adaptive algorithm starting from a structured triangular initial mesh which is far too coarse to be able to resolve the solution's sharp interior layer. The meshes sequence clearly show the effectiveness of the estimator in capturing the areas where the error is higher.

5.3. Test 3. Convection-dominated problem: boundary layer

Here we consider $\Omega := (0, 1)^2$ with data $\boldsymbol{\kappa} = \begin{pmatrix} 1 & 0 \\ 0 & 1 \end{pmatrix}$, $\mathbf{b} = \begin{pmatrix} 1 \\ 1 \end{pmatrix}$, and $\gamma = 0$, whereas the source term f is such that the exact solution is given by

$$u(x, y) = \sin\left(\frac{\pi x}{2}\right) + \sin\left(\frac{\pi y}{2}\right)\left(1 - \sin\left(\frac{\pi x}{2}\right)\right) + \frac{e^{-1/\epsilon} - e^{-(1-x)(1-y)/\epsilon}}{1 - e^{-1/\epsilon}}.$$

Notice that the solution is non-zero at the boundary. Moreover, for small ϵ, the solution possesses boundary layers along the boundaries $x = 1$ and $y = 1$ (see Fig. 5.7). For this test we use $\epsilon = 10^{-3}$. From Fig. 5.8 it is possible to observe how the expected order of convergence is reached after a few iterations of the adaptive algorithm. Some intermediate meshes obtained by the adaptive algorithm are displayed in Fig. 5.9. Here we notice that the adapted meshes concentrate the refinements along the lines $x = 1$ and $y = 1$.

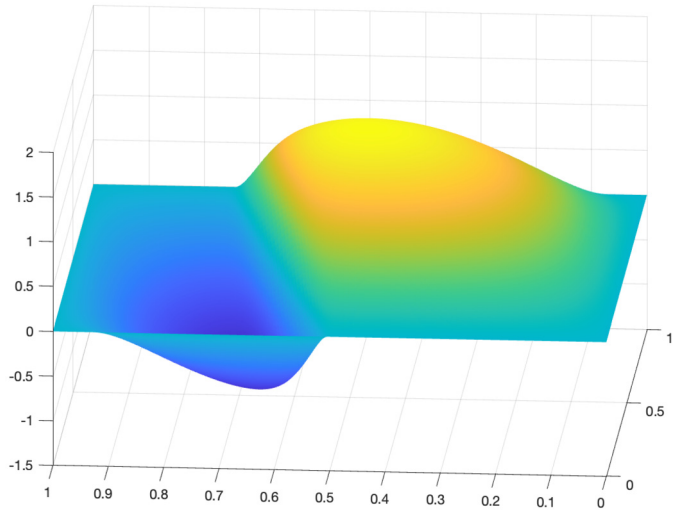

Fig. 5.3. Test 2. Exact solution.

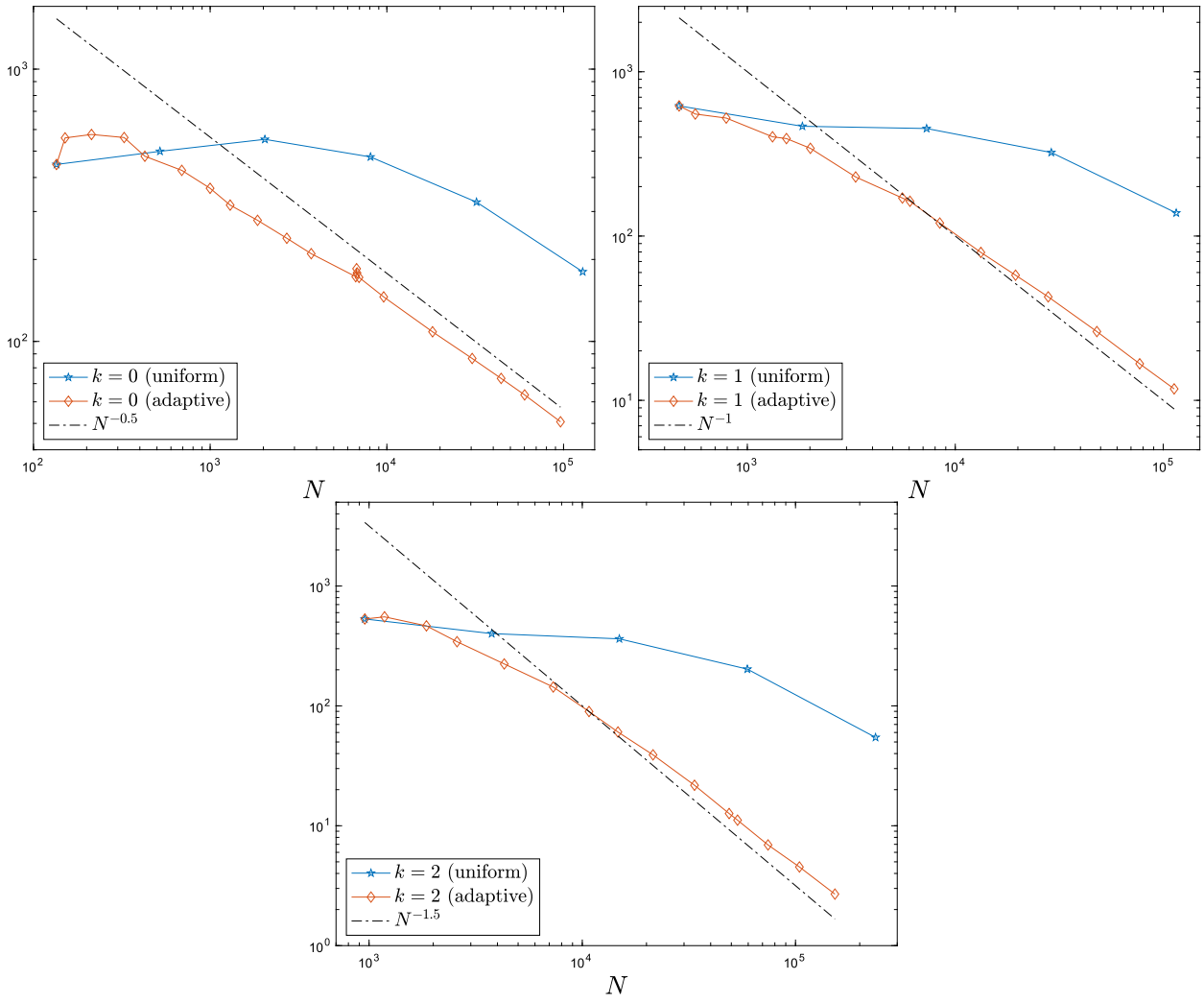

Fig. 5.4. Test 2. Error curves under uniform and adaptive refinement of the error $\mathsf{e}(\boldsymbol{\sigma}, u)$ using the estimator $\boldsymbol{\eta}$ and meshes composed of triangles.

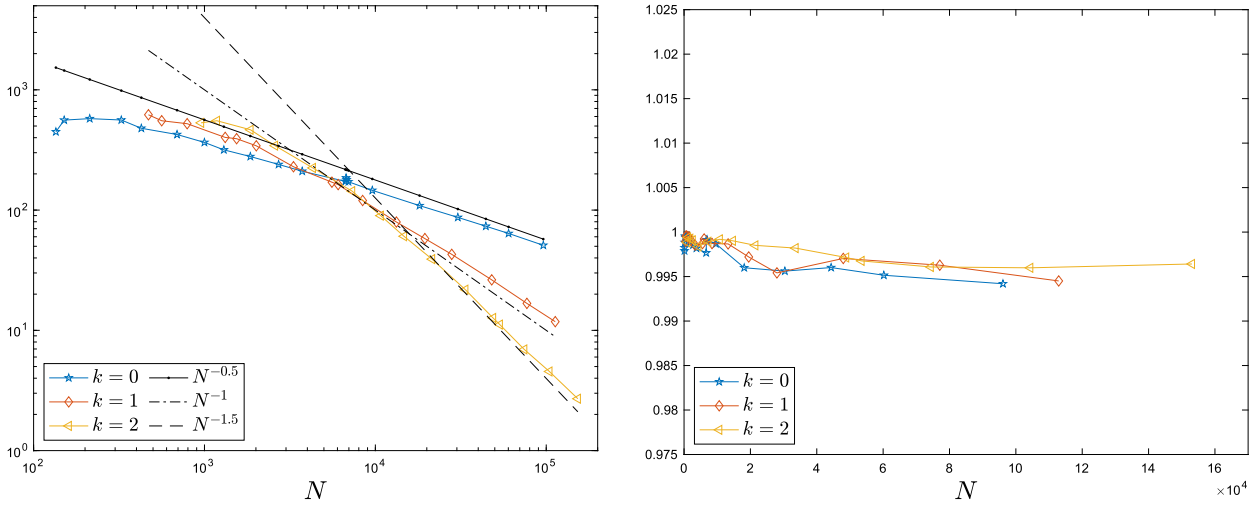

Fig. 5.5. Test 2. Behaviour under adaptive refinement (left). Effectivity of the estimator (right).

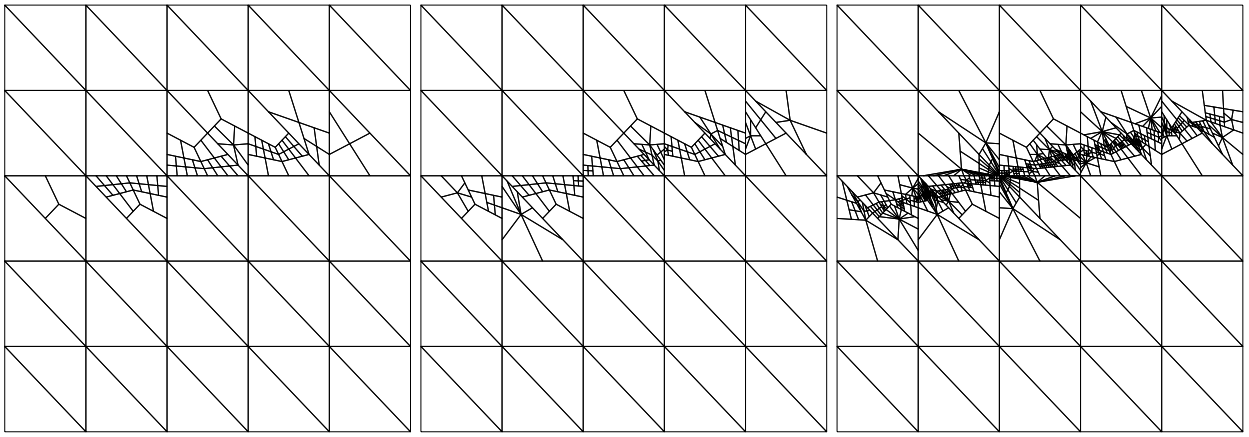

Fig. 5.6. Test 2. Some meshes from the adaptive refinement sequence obtained with $k = 1$: after 3 refinement steps (left), after 5 refinement steps (centre), and after 9 refinement steps (right).

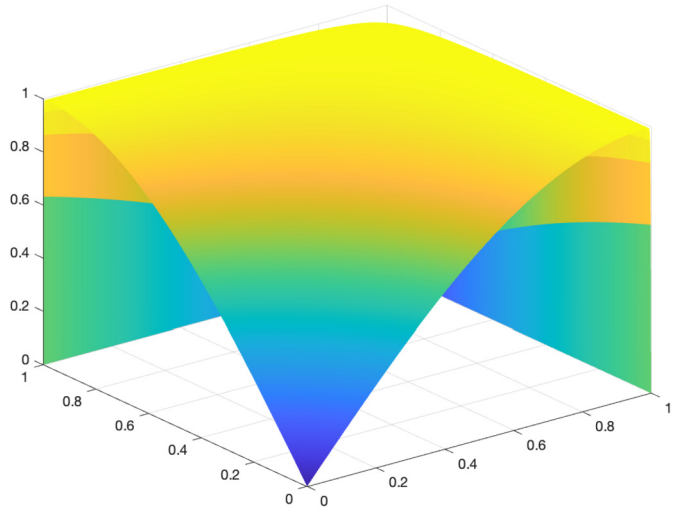

Fig. 5.7. Test 3. Exact solution.

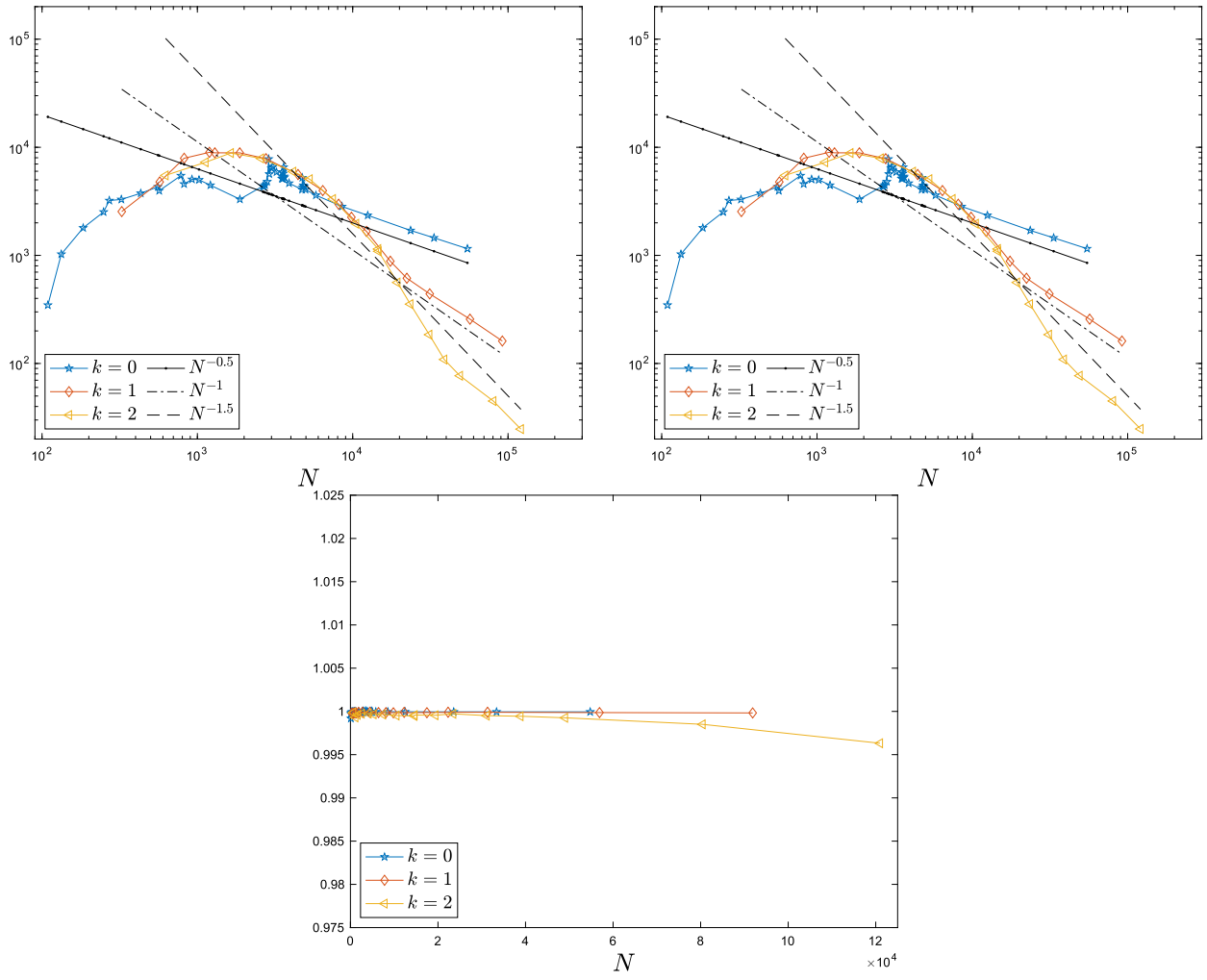

Fig. 5.8. Test 3. Top. Convergence under adaptive refinement of the error $\mathsf{e}(\boldsymbol{\sigma}, u)$ (top-left) and the estimator (top-right). Effectivity of the estimator (bottom).

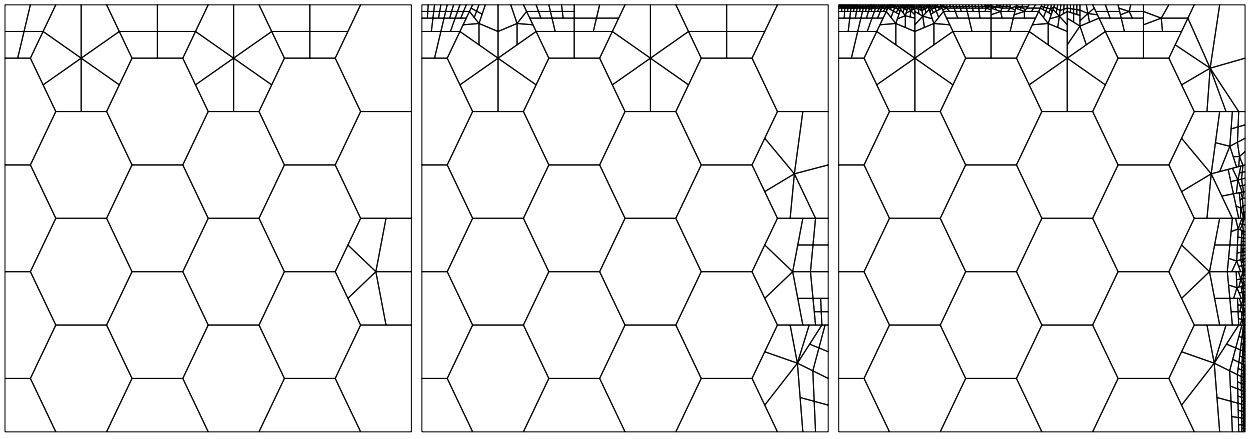

Fig. 5.9. Test 3. Some meshes from the adaptive refinement sequence obtained with $k = 1$: after 1 refinement steps (left), after 4 refinement steps (centre), and after 9 refinement steps (right).

5.4. Test 4. Interior layer with variable data

We consider the test from [38] but characterised by the data:

$$\boldsymbol{\kappa} = \begin{pmatrix} y^2+1 & -xy \\ -xy & x^2+1 \end{pmatrix}, \quad \mathbf{b} = \begin{pmatrix} x \\ y \end{pmatrix}, \quad \text{and} \quad \gamma = x^2 + y^3,$$

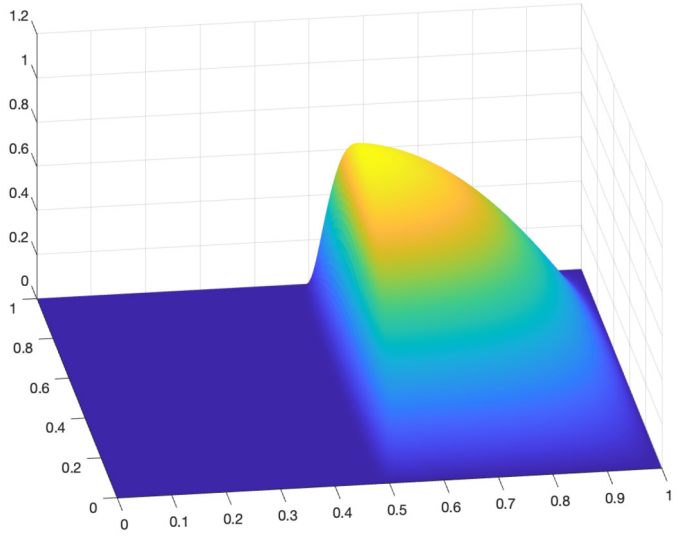

Fig. 5.10. Test 4. Exact solution.

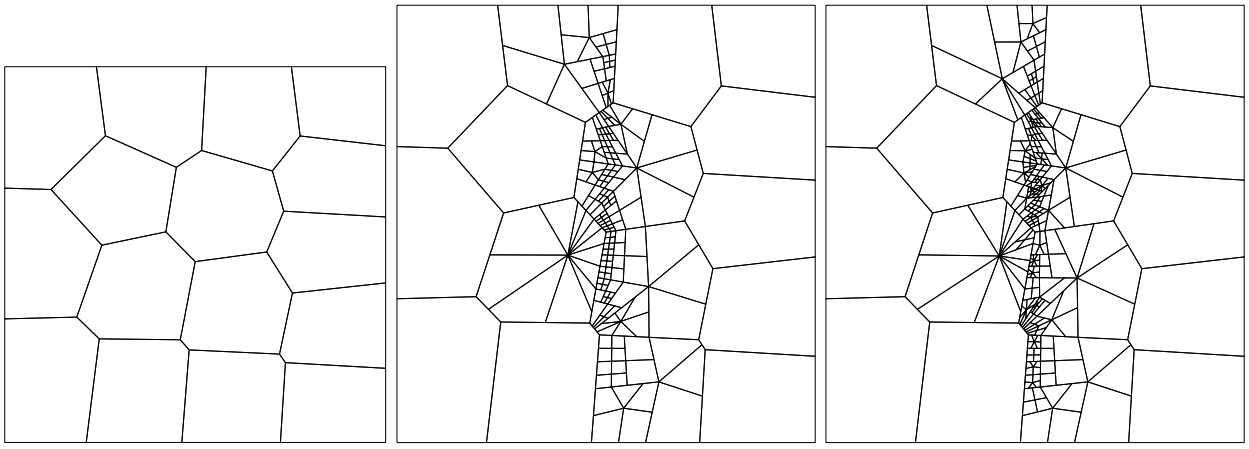

Fig. 5.11. Test 4. Some meshes from the adaptive refinement sequence for $k = 1$: initial mesh (left), 4 refinement steps (centre), and 8 refinement steps (right).

whereas the source term f is such that the exact solution is given by

$$u(x, y) = \frac{25}{3} xy(1 - x)(1 - y) \left(1 - \tanh \frac{\alpha - x}{\xi}\right)$$

Here we choose the parameters $\alpha = 0.5$ and $\xi = 0.01$ (Fig. 5.10). The solution has an interior layer which is once again correctly captured by the adaptive algorithm as evidenced by the meshes reported in Fig. 5.11. The adaptive algorithm's convergence history and the effectivity of the estimator are presented in the Fig. 5.12. Once again, the estimator is seen to converge optimally with bounded effectivity. We remark here that we use different β in the adaptive algorithm due to the polynomial order effect. More precisely, we use $\beta = 0.5$ for $k = 0$ whereas $\beta = 0.7$ was used for $k = 1, 2$. If the adaptive algorithm has a small beta value, it will over-refine the mesh, requiring more refinement steps to stabilize the estimator effectiveness.

6. Conclusions and extensions

We have derived a posteriori error estimates for a mixed-VEM approach for a second order elliptic equation in divergence form. We have proved upper and lower bounds for the error between the true solution and a computable postprocessing of the VEM approximation. Arguments based in the inf-sup global condition, suitable Helmholtz decompositions and a type Clément-type interpolant were used to derive the upper bound. The lower bound was obtained, in classical fashion, by using localisation techniques of bubble functions. We have also proposed an adaptive algorithm based on the fully local and computable error estimator derived from the a posteriori error analysis. Its performance and effectiveness was illustrated through some numerical test. The extension of the present analysis including a posteriori error estimates in the case of anisotropic meshes will be the subject of future works.

Data availability

No data was used for the research described in the article.

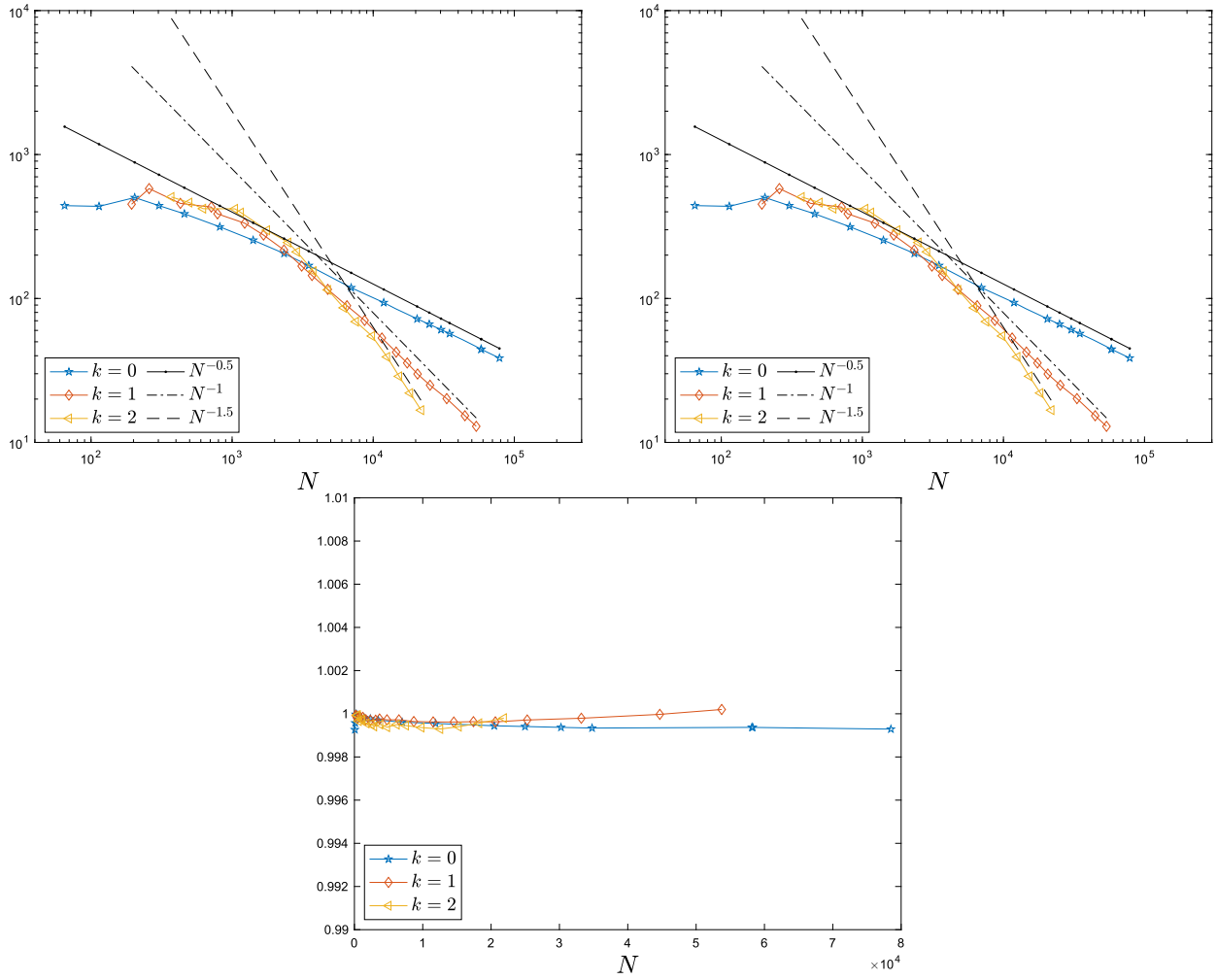

Fig. 5.12. Test 4. Convergence under adaptive refinement of the error $\mathfrak{e}(\boldsymbol{\sigma}, u)$ (top-left) and the estimator (top-right). Effectivity of the estimator (bottom).

References

[1] B. Adams, T. Olson, The mesostructure-properties linkage in polycrystals, Prog. Mater. Sci. 43 (1998) 1–88.
[2] P. Adler, J. Thovert, Fractures and Fracture Networks, Kluwer Academic, Dordrecht, 1999.
[3] P.F. Antonietti, S. Berrone, A. Borio, A. D'Auria, M. Verani, S. Weisser, Anisotropic *a posteriori* error estimate for the virtual element method, IMA J. Numer. Anal. 42 (2022) 1273–1312.
[4] T.P. Barrios, G.N. Gatica, M.a. González, N. Heuer, A residual based a posteriori error estimator for an augmented mixed finite element method in linear elasticity, ESAIM: Math. Model. Numer. Anal. 40 (2006) 843–869.
[5] L. Beirão da Veiga, F. Brezzi, A. Cangiani, G. Manzini, L. Marini, A. Russo, Basic principles of virtual element methods, Math. Models Methods Appl. Sci. 23 (2013) 199–214.
[6] L. Beirão da Veiga, F. Brezzi, L. Marini, A. Russo, Mixed virtual element methods for general second order elliptic problems on polygonal meshes, ESAIM: Math. Model. Numer. Anal. 50 (2016) 727–747.
[7] L. Beirão da Veiga, K. Lipnikov, G. Manzini, The Mimetic Finite Difference Method for Elliptic Problems, MS&A. Modeling, Simulation and Applications, vol. 11, Springer, Cham, 2014.
[8] L. Beirão da Veiga, G. Manzini, Residual *a posteriori* error estimation for the virtual element method for elliptic problems, ESAIM: Math. Model. Numer. Anal. 49 (2015) 577–599.
[9] L. Beirão da Veiga, G. Manzini, L. Mascotto, A posteriori error estimation and adaptivity in *hp* virtual elements, Numer. Math. 143 (2019) 139–175.
[10] S. Berrone, A. Borio, A residual *a posteriori* error estimate for the Virtual Element Method, Math. Models Methods Appl. Sci. 27 (2017) 1423–1458.
[11] S. Berrone, A. Borio, A. D'Auria, Refinement strategies for polygonal meshes applied to adaptive VEM discretization, Finite Elem. Anal. Des. 186 (2021) 103502, 16.
[12] S.C. Brenner, L.R. Scott, The Mathematical Theory of Finite Element Methods, third ed., Texts in Applied Mathematics, vol. 15, Springer, New York, 2008.
[13] E. Cáceres, G.N. Gatica, F.A. Sequeira, A mixed virtual element method for the Brinkman problem, Math. Models Methods Appl. Sci. 27 (2017) 707–743.
[14] A. Cangiani, Z. Dong, E.H. Georgoulis, P. Houston, *hp*-Version Discontinuous Galerkin Methods on Polygonal and Polyhedral Meshes, SpringerBriefs in Mathematics, Springer, Cham, 2017.
[15] A. Cangiani, E.H. Georgoulis, T. Pryer, O.J. Sutton, A posteriori error estimates for the virtual element method, Numer. Math. 137 (2017) 857–893.
[16] A. Cangiani, M. Munar, A posteriori error estimates for mixed virtual element methods, https://arxiv.org/abs/1904.10054.
[17] S. Cao, L. Chen, Anisotropic error estimates of the linear nonconforming virtual element methods, SIAM J. Numer. Anal. 57 (2019) 1058–1081.
[18] C. Carstensen, A posteriori error estimate for the mixed finite element method, Math. Comput. 66 (1997) 465–476.
[19] H. Chi, L. Beirão da Veiga, G.H. Paulino, A simple and effective gradient recovery scheme and *a posteriori* error estimator for the virtual element method (VEM), Comput. Methods Appl. Mech. Eng. 347 (2019) 21–58.
[20] M. Cicuttin, A. Ern, N. Pignet, Hybrid High-Order Methods—A Primer with Applications to Solid Mechanics, SpringerBriefs in Mathematics, Springer, Cham, 2021, ©2021.
[21] D. Copeland, U. Langer, D. Pusch, From the boundary element domain decomposition methods to local Trefftz finite element methods on polyhedral meshes, in: Domain Decomposition Methods in Science and Engineering XVIII, in: Lect. Notes Comput. Sci. Eng., vol. 70, Springer, Berlin, 2009, pp. 315–322.
[22] L.B. da Veiga, C. Canuto, R.H. Nochetto, G. Vacca, M. Verani, Adaptive vem: stabilization-free a posteriori error analysis, https://arxiv.org/abs/2111.07656.
[23] A.R. Diaz, A. Bénard, Designing materials with prescribed elastic properties using polygonal cells, Int. J. Numer. Methods Eng. 57 (2003) 301–314.
[24] G.N. Gatica, A note on the efficiency of residual-based a-posteriori error estimators for some mixed finite element methods, Electron. Trans. Numer. Anal. 17 (2004) 218–233.

[25] G.N. Gatica, L.F. Gatica, F.A. Sequeira, Analysis of an augmented pseudostress-based mixed formulation for a nonlinear Brinkman model of porous media flow, Comput. Methods Appl. Mech. Eng. 289 (2015) 104–130.
[26] G.N. Gatica, A. Márquez, M.A. Sánchez, Analysis of a velocity-pressure-pseudostress formulation for the stationary Stokes equations, Comput. Methods Appl. Mech. Eng. 199 (2010) 1064–1079.
[27] G.N. Gatica, M. Munar, F.A. Sequeira, A mixed virtual element method for a nonlinear Brinkman model of porous media flow, Calcolo 55 (2018) 21, 36.
[28] F. Lepe, D. Mora, G. Rivera, I. Velásquez, A posteriori virtual element method for the acoustic vibration problem, Adv. Comput. Math. 49 (2023) 23, 1.
[29] D. Mora, G. Rivera, A priori and a posteriori error estimates for a virtual element spectral analysis for the elasticity equations, IMA J. Numer. Anal. 40 (2020) 322–357.
[30] D. Mora, G. Rivera, R. Rodríguez, A posteriori error estimates for a Virtual Element Method for the Steklov eigenvalue problem, Comput. Math. Appl. 74 (2017) 2172–2190.
[31] M. Munar, F.A. Sequeira, A posteriori error analysis of a mixed virtual element method for a nonlinear Brinkman model of porous media flow, Comput. Math. Appl. 80 (2020) 1240–1259.
[32] S. Rjasanow, S. Weißer, Higher order BEM-based FEM on polygonal meshes, SIAM J. Numer. Anal. 50 (2012) 2357–2378.
[33] N. Sukumar, A. Tabarraei, Conforming polygonal finite elements, Int. J. Numer. Methods Eng. 61 (2004) 2045–2066.
[34] R. Verfurth, A Review of A Posteriori Error Estimation and Adaptive Mesh-Refinement Techniques, Wiley - Teubner, 1996.
[35] E.L. Wachspress, A rational basis for function approximation, J. Inst. Math. Appl. 8 (1971) 57–68.
[36] G. Wang, J. Meng, Y. Wang, L. Mei, *A priori* and *a posteriori error* estimates for a virtual element method for the non-self-adjoint Steklov eigenvalue problem, IMA J. Numer. Anal. 42 (2022) 3675–3710.
[37] G. Wang, Y. Wang, Y. He, A posteriori error estimates for the virtual element method for the Stokes problem, J. Sci. Comput. 84 (2020) 37, 25.
[38] G. Wang, Y. Wang, Y. He, Least-squares virtual element method for the convection-diffusion-reaction problem, Int. J. Numer. Methods Eng. 122 (2021) 2672–2693.